



**HAL**  
open science

## **The influence of synoptic circulations and local processes on temperature anomalies at three French observatories.**

Cheikh Dione, Fabienne Lohou, Marjolaine Chiriaco, Marie Lothon, Sophie Bastin,  
Jean-Luc Baray, Pascal Yiou, Aurélie Colomb

### ► **To cite this version:**

Cheikh Dione, Fabienne Lohou, Marjolaine Chiriaco, Marie Lothon, Sophie Bastin, et al.. The influence of synoptic circulations and local processes on temperature anomalies at three French observatories.. *Journal of Applied Meteorology and Climatology*, 2017, 58 (1), pp.141-158. <10.1175/JAMC-D-16-0113.1>. <hal-01372848v2>

**HAL Id: hal-01372848**

**<https://insu.hal.science/hal-01372848v2>**

Submitted on 26 Jun 2017

**HAL** is a multi-disciplinary open access archive for the deposit and dissemination of scientific research documents, whether they are published or not. The documents may come from teaching and research institutions in France or abroad, or from public or private research centers.

L'archive ouverte pluridisciplinaire **HAL**, est destinée au dépôt et à la diffusion de documents scientifiques de niveau recherche, publiés ou non, émanant des établissements d'enseignement et de recherche français ou étrangers, des laboratoires publics ou privés.



Distributed under a Creative Commons CC BY-NC-ND 4.0 - Attribution - Non-commercial use - No Derivative Works - International License



1 **The influence of synoptic circulations and local processes on temperature**  
2 **anomalies at three French observatories**

3 Cheikh DIONE<sup>1\*†</sup>, Fabienne LOHOU<sup>1</sup>, Marjolaine CHIRIACO<sup>2</sup>, Marie LOTHON<sup>1</sup>, Sophie  
4 BASTIN<sup>2</sup>, Jean-Luc BARAY<sup>3</sup>, Pascal YIOU<sup>4</sup> and Aurélie COLOMB<sup>3</sup>

5 *(1) Laboratoire d'Aérodologie, Université de Toulouse, CNRS, UPS, France.*

6 *(2) LATMOS/IPSL, UVSQ Université Paris-Saclay, UPMC Univ. Paris 06, CNRS, Guyancourt,*  
7 *France.*

8 *(3) Laboratoire de Météorologie Physique, UMR 6016 Université Blaise Pascal/CNRS, Clermont*  
9 *Ferrand, France.*

10 *(4) Laboratoire des Sciences du Climat et de l'Environnement, UMR8212 CEA-CNRS-UVSQ,*  
11 *Université Paris - Saclay & IPSL, Gif-Sur-Yvette, France.*

12 *\*Corresponding author address: Dr. Cheikh DIONE, Centre de Recherches Atmosphériques, 8*  
13 *route de Lannemezan, 65300 Campistrous, France.*

14 *E-mail: Cheikh.dione@aero.obs-mip.fr*

15 *†Current affiliation: Laboratoire d'Aérodologie, Université de Toulouse, CNRS, UPS, France.*

## ABSTRACT

16 The relative contribution of the synoptic-scale circulations to local and  
17 mesoscale processes was quantified in terms of the variability of middle lat-  
18 itude temperature anomalies from 2003 to 2013 using meteorological vari-  
19 ables collected from three French observatories and reanalyses. Four weather  
20 regimes were defined from sea level pressure anomalies using National Center  
21 for Environmental Prediction (NCEP) reanalyses with a K-means algorithm.  
22 No correlation was found between daily temperature anomalies and weather  
23 regimes, and the variability of temperature anomalies within each regime was  
24 large. It was therefore not possible to evaluate the effect of large scales on  
25 temperature anomalies by this method. An alternative approach was found  
26 with the use of the analogues method: the principle being that for each day of  
27 the considered time series, a set of days which had a similar large-scale 500  
28 hPa geopotential height field within a fixed domain were considered. The ob-  
29 served temperature anomalies were then compared to those observed during  
30 the analogue days: the closer the two types of series, the greater the mark of  
31 the large scale. This method highlights a widely predominant influence of the  
32 large-scale atmospheric circulation on the temperature anomalies. It showed a  
33 potentially larger influence of the Mediterranean Sea and orographic flow on  
34 the two southern observatories. Low-level cloud radiative effects substantially  
35 modulated the variability of the daily temperature anomalies.

## 36 **1. Introduction**

37 Temperature fluctuations in France and, more generally, Western European are largely connected  
38 to large-scale weather regimes. However, the processes linking atmospheric variability to surface  
39 temperature may vary with the season. Cattiaux et al. (2010) used 500 hPa geopotential height to  
40 define weather regimes influencing Europe and found that the cold winter of 2010 was associated  
41 with a large occurrence of the negative phase of the North Atlantic Oscillation (NAO) weather  
42 regime. In summer, major heat waves over France and the UK are generally linked to persistent  
43 anticyclonic conditions (such as those in 2003) (Cassou et al. 2005; Yiou et al. 2008). They  
44 may also be linked to Atlantic low pressure, which leads to southerly flows (such as those seen  
45 in 2015), with amplification by soil moisture-temperature and boundary-layer feedbacks (Schär  
46 et al. 2004; Seneviratne et al. 2006; Fischer et al. 2007b; Vautard et al. 2007; Quesada et al. 2012;  
47 Miralles et al. 2014). Warm winters are linked to a zonal westerly flow (such as in 2007 and 2014)  
48 (Luterbacher et al. 2007), which can be amplified by land albedo and cloud radiative effects. The  
49 role of such amplifying factors was investigated mainly with regional model simulations (Zampieri  
50 et al. 2009; Stegehuis et al. 2013; Seneviratne et al. 2004; Stefanon et al. 2014), but it was proven  
51 necessary to use high-resolution observations to validate such an approach, since models seemed  
52 to exacerbate the role of these factors over Europe (Cheruy et al. 2014; Bastin et al. 2016). For  
53 example, Chiriaco et al. (2014), using a combination of space and ground-based observations and  
54 twin simulations, showed that the heat wave that occurred over Northern Europe in July 2006  
55 was linked to specific large-scale conditions favoring a low cloud deficit over this area and was  
56 amplified by dry soil, which contributed to about 40% of the anomaly.

57 As for the weather regimes, a flow analogue method was also used to study the seasonal vari-  
58 ability of surface temperature anomalies over Europe (Cattiaux et al. 2010; Chiriaco et al. 2014;

59 Vautard and Yiou 2009; Yiou et al. 2007). Cattiaux et al. (2010) found a larger positive depar-  
60 ture of observed temperatures from flow analogues for minimum than for maximum temperatures.  
61 They observed a maximum departure over the Alps region. Spatial variability and underestimation  
62 of observed temperature anomalies by reconstructed temperature anomalies suggest an important  
63 role of the smaller scale processes concerning temperature anomalies. France is located in a tran-  
64 sitional region between subtropical influences and Atlantic perturbations. It covers an area where  
65 climatic model predictions have suggest significant uncertainty, with large scatter in temperature  
66 and precipitation due to different sensitivities to local processes (Boé and Terray 2014). For these  
67 reasons, it is useful to employ observational data to quantify the influence of large-scale atmo-  
68 spheric circulations relative to those of local processes to help explain the variability of daily  
69 temperature anomalies across France.

70 Our study aims to quantify the relative contributions of large-scale atmospheric circulations and  
71 of local processes on the variability of temperature anomalies at three observatories located in  
72 France. For this, we shall evaluate specific issues : (i) the effect of weather regimes on daily tem-  
73 perature anomalies by use of the classification of weather regimes defined from sea level pressure  
74 (Yiou and Nogaj 2004), and (ii) the capability of local processes to amplify or reduce temperature  
75 anomalies by use of flow analogue atmospheric circulations based on geopotential height at 500  
76 hPa (Yiou et al. 2007). Our analysis is based on a series of meteorological variables (temperature,  
77 wind and radiation) observed at three observatories from ROSEA (Réseau d’Observatoires pour  
78 la Surveillance de l’Eau Atmosphérique) national network. It is also based on reanalyses (NCEP  
79 and ECMWF).

80 The manuscript is organized as follows. In section 2, the three ROSEA observatories, the cor-  
81 responding datasets, the large-scale diagnostic and the methodological approach are presented.

82 Section 3 presents the analysis of large-scale conditions versus local processes using flow ana-  
83 logues. Conclusions appear in section 4.

## 84 **2. Data and methodology**

### 85 *a. Observatories*

86 In this study, we use surface observations from three observatories (SIRTA (Site Instrumen-  
87 tal de Recherche en Télédetection Active), COPDD (Cézeaux-Opme-Puy De Dôme) and P2OA  
88 (Plateforme Pyrénéenne de l'Observation de l'Atmosphère)) from the five ROSEA network ob-  
89 servatories, located across varied landscapes along a North-South transect across France (Figs. 1a  
90 and 1b).

#### 91 1) SIRTA

92 The northern observatory of ROSEA is known as SIRTA (48.7°N-2.2°E and 160 m elevation)  
93 (Haeffelin 2005). SIRTA is located on a plateau in a suburban area in Palaiseau, 20 km south-  
94 west of Paris (Fig. 1a). It is dedicated to the research of physical and chemical processes in the  
95 atmosphere, mainly using remote sensing. Since 2002, observations of precipitation, water va-  
96 por, clouds, meteorological variables, atmospheric gases, solar radiation, and wind power have  
97 been collected. More details concerning the SIRTA observatory can be found in Haeffelin (2005)  
98 or on the following website: <http://sirta.ipsl.polytechnique.fr/sirta.old/>. Quality control and ho-  
99 mogenization of the data yielding a uniform hourly time-resolution was undertaken at SIRTA for  
100 the entire observation period (Chiriaco et al. 2014; Cheruy et al. 2013). This project, named  
101 SIRTA-ReOBS, provides a single netCDF file with more than 40 variables from 2003 to 2013  
102 (<http://sirta.ipsl.polytechnique.fr/sirta.old/reobs.html>).

## 103 2) CÉZEAUX-COPDD

104 The COPDD observatory is located in the Auvergne region, in the center of France (Fig. 1a)  
105 where various in situ and remote sensing instruments continuously measure the atmospheric dy-  
106 namics, radiation, atmospheric gases, cloud microphysical variables and aerosols. This observa-  
107 tory is composed of three instrumented sites: Cézeaux (at an altitude of 394 m, an urban site,  
108 Opme (at an altitude of 680 m), and Puy-De-Dôme (at an altitude of 1465 m). In this study, we  
109 use the meteorological variables collected at the Cézeaux site in order to obtain relatively similar  
110 terrain across the three sites. The Cézeaux site (45.47°N-3.05°E) is located on a plain on the cam-  
111 pus of Blaise Pascal University in Clermont Ferrand. Since 2002, meteorological variables have  
112 been measured at this site. More details concerning the COPDD observatory can be found on the  
113 following website; <http://wwwobs.univ-bpclermont.fr/SO/mesures/index.php>.

## 114 3) CRA-P2OA

115 The P2OA observatory is the southern most site (Fig. 1a). It is located in the Midi-Pyrénées  
116 region and is composed of two sites from the Observatoire Midi Pyrénées (OMP): the Atmo-  
117 spheric Research Center (CRA) in Lannemezan (43.13°N-0.369°E at an altitude of 600 m), and  
118 the “Pic du Midi” (43.13°N-0.37°E at an altitude of 2877 m). On this platform, various in situ  
119 and remote sensing instruments continuously measure the atmospheric dynamics, surface energy  
120 balance, radiation, chemistry, aerosols and atmospheric electricity. Here, we use only meteorolog-  
121 ical observations at the CRA site which is a rural site located on a plateau in the foothills of the  
122 Pyrenees. At the CRA site, standard meteorological observations have been collected since 1995.  
123 More details on the P2OA observatory can be found on the website <http://p2oa.aero.obs-mip.fr/>.

124 Given the geographical position of the three observatories, various local processes, such as urban  
125 heat islands, cloud cover, and mountain/plain breeze circulations, snow cover, and clouds have a  
126 role to play concerning daily temperature anomalies.

### 127 *b. Data used*

128 In order to base our analysis on a common period with a uniform data format, data from the  
129 Meteo-France standard weather station hosted by CRA-P2OA were used for this study. We em-  
130 ployed hourly values concerning temperature and incoming shortwave radiation at 2 m, wind speed  
131 and direction at 10 m and rainfall between 2003 and 2013. In the framework of the current study,  
132 a similar quality control, homogenization and a combination of variables from various sources  
133 as seen in the SIRTA-ReOBS were performed for the meteorological variables collected in the  
134 Cézeaux-COPDD and CRA-P2OA observatories.

135 To characterize the influence of large-scale circulations, we based our study mainly on daily  
136 temperature anomalies at 2 m above the surface at the three observatories. To ensure that our  
137 anomaly was not affected by seasonal variability in temperatures, it was defined by comparison  
138 to the average of the current month. We defined the daily temperature anomalies ( $aT(j)$ ) for the  
139 day  $j$  by removing the 2003-2013 monthly mean temperature at each observatory. This can be  
140 expressed through the following equation:

$$aT(j) = \langle T \rangle_j - \langle T \rangle_{[m,2003-2013]} \quad (1)$$

141 where  $\langle T \rangle_j$  is the daily mean temperature for the day  $j$ , computed from the mean of hourly tem-  
142 peratures.  $\langle T \rangle_{[m,2003-2013]}$  is the monthly mean temperature calculated over the entire period,  
143 and  $m$  is the month represented numerically. For example,  $\langle T \rangle_{[1,2003-2013]}$  was the temperature  
144 averaged over all the days in January across the period 2003-2013.

145 *c. Large scale analysis diagnostics*

146 1) WEATHER REGIMES

147 Weather regimes enable us to describe large-scale atmospheric circulations in a simple man-  
148 ner. With this in mind, we used the classification of weather regimes used by Yiou and Nogaj  
149 (2004) and based on the daily anomalies of sea level pressure (SLP) acquired from the NCEP (Na-  
150 tional Center for Environmental Prediction) reanalyses ( $2.5^\circ \times 2.5^\circ$ ) (Kalnay 1996). The weather  
151 regimes are defined in the Euro-Atlantic region ( $80^\circ\text{W}$ - $30^\circ\text{E}$ ,  $30$ - $70^\circ\text{N}$ ) (Fig. 1b, (the larger black  
152 square one) and determined from the “K-means” algorithm, computed from the first 10 Empirical  
153 Orthogonal Functions (EOFs) of seasonal SLP anomalies (Cheng and Wallace 1993; Michelan-  
154 geli et al. 1995) from 1948 to 2014. The classification used in this study therefore depends on the  
155 season. Figure 2 illustrates the four weather regimes defined in winter and their occurrence during  
156 the 1948-2014 period. We note in this Figure, the positive (reg. 3) and negative (reg. 4) phases of  
157 the North Atlantic Oscillation (respectively  $\text{NAO}^+$  and  $\text{NAO}^-$ ), a “Scandinavian blocking” (reg.  
158 2), and the “Atlantic Ridge” (reg. 1). Weather regimes appear with a similar frequency with a 27%  
159 occurrence for  $\text{NAO}^+$  and “Scandinavian blocking”. During the transitional seasons of spring and  
160 autumn, a classification into weather regimes is not always appropriate due to seasonal shifts (Vrac  
161 et al. 2013). Vrac et al. (2013) found that spring frequently corresponds to an early summer or a  
162 longer winter, and that autumn is related to a longer summer or earlier winter, making a definition  
163 of a regime during these two seasons difficult. Here, we do not consider this classification for  
164 transitional seasons. It is also necessary to consider the stability of the regimes during the winter  
165 and summer, as they are sometimes not well defined, and only transitory.

166 In order to eliminate the days with ambiguous classification in winter and summer, we use a  
167 criterion based on the Euclidean distance and the spatial correlation from the nearest weather

168 regime deduced by the K-means method. We filter the classification by eliminating the days for  
169 which the Euclidean distance from the nearest weather regime is larger than 10 hPa and with a  
170 spatial correlation with the nearest weather regime lower than 0.15. We eliminated 5.2% (52 days)  
171 and 10,8% (109 days) of the total days in winter and summer respectively.

172 Here, we are interested in the influence of the large-scale atmospheric regimes on the variabil-  
173 ity of daily temperature anomalies (equation 1) at the three observatories. Figure 3 shows the  
174 box plot of daily temperature anomalies in winter and summer for each site and for each weather  
175 regime during the 2003-2013 period. This Figure indicates that in winter,  $NAO^+$  yields relatively  
176 milder temperatures at all sites, while  $NAO^-$  and blocking are characterized by relatively colder  
177 temperatures at all sites. During Atlantic Ridge conditions, the occurrence of either warmer or  
178 colder temperatures than those on average is relatively similar, except at SIRTA, where the winter  
179 is mostly mild when this regime prevails. It is however, important to note that specific anomalies,  
180 warm or cold, can occur whatever the weather regime at SIRTA, whilst very cold winter days are  
181 unlikely to occur at Cézeaux-COPDD or CRA-P2OA when  $NAO^+$  or Atlantic Ridge conditions  
182 exist. Extreme temperature anomalies are more frequent at SIRTA, and variability is usually en-  
183 hanced, except during  $NAO^+$ . In summer, the weather regimes have almost the same effect at all  
184 sites, even if the variability at Cézeaux-COPDD is greater than at the other two sites, and extremes  
185 are enhanced. At Cézeaux-COPDD, the Atlantic Ridge and  $NAO^+$  have positive daily anomalies  
186 on average in winter ( $0.6\text{ }^\circ\text{C}$  and  $0.2\text{ }^\circ\text{C}$  respectively) and summer ( $0.6\text{ }^\circ\text{C}$  and  $1.9\text{ }^\circ\text{C}$  respectively),  
187 indicating mild and warm temperatures respectively during these two seasons. These results are  
188 consistent with those of Yiou et al. (2007) in the fall/winter of 2006/2007. From these results, we  
189 conclude that the weather regimes derived from the SLP data do not explain the daily temperature  
190 anomalies at the three observatories in winter and summer.

## 191 2) LARGE-SCALE FLOW ANALOGUES

192 The slight difference in the anomaly of mean temperatures among the weather regimes in sum-  
193 mer, the large variability in the daily temperature anomalies and the fact that the weather regimes  
194 are not easily defined in spring and autumn, motivated us to augment the regime approach with  
195 the flow-analogue method.

196 The method of atmospheric flow analogues was first introduced by Lorenz (1969). Since then, it  
197 has found many applications, including weather prediction (Van den Dool 2007). Yiou et al. (2007)  
198 used this approach to infer the connection between surface climate variables and atmospheric  
199 circulation. In this study, we use the flow-analogue method developed by Yiou et al. (2007) and  
200 used by Chiriaco et al. (2014) and Cattiaux et al. (2010) to study climate variability across Europe.  
201 For each day during the eleven year period (2003-2013), we looked for days within the same  
202 time series which had similar large-scale atmospheric conditions. For this, we considered field  
203 anomalies of geopotential height at 500 hPa from the ERA-Interim (ERA-Interim) reanalyses ( $0.75^\circ \times$   
204  $0.75^\circ$ ) of European Center for Medium-Range Weather Forecasts (ECMWF) (Dee et al. 2011), a  
205 typical diagnostic tool for large-scale circulations. Analogue days were found by minimizing a  
206 Euclidean distance and maximizing a Spearman correlation. More details on the flow analogues  
207 method can be found in Yiou et al. (2007).

208 By using flow analogues to quantify the relative influence of the large, local, and mesoscale  
209 processes on surface temperature anomalies, we considered two nested domains. The first domain  
210 covers the Euro-Atlantic region ( $80^\circ\text{W}$ - $30^\circ\text{E}$ ,  $30^\circ\text{N}$ - $70^\circ\text{N}$ ) (Fig. 1b, black square). This domain  
211 is also the one used by Cattiaux et al. (2010); Vautard and Yiou (2009); Yiou et al. (2007) and  
212 Chiriaco et al. (2014) to establish the link between extreme events (cold waves, heat waves and  
213 drought) and large-scale conditions over Europe. The second domain covers the area  $21^\circ\text{W}$ - $30^\circ\text{E}$ ,

214 30-60°N (Fig. 1b, white square). Compared to the larger domain, this smaller domain (mesoscale)  
215 weighs the influence of the Mediterranean sea on synoptic circulations more heavily than the  
216 Atlantic Ocean.

217 For each day in our studied period and for each domain considered, we kept a maximum of ten  
218 analogues, which satisfied the following two criteria: (i) the Spearman spatial correlation had to be  
219 greater or equal to 0.6, ensuring the quality of the similarity, and (ii) they should not be closer than  
220 6 days from the current day, in order to ensure that the analogues were independent of the target  
221 day (assuming a decorrelation time of 3 days before and 5 days after the target day). These criteria  
222 eliminated 6,4 % (around 256 days) of the days from the large domain and 3 % (around 119 days)  
223 from the small domain. The scores are higher in winter, spring and autumn than in summer for  
224 both domains. We found 134 and 54 unselected days respectively for the large and small domain  
225 in Summer.

#### 226 *d. Analysis protocol*

227 To quantify the contribution of local processes and large scale circulations at each site, we com-  
228 pared the observed temperature anomalies to the temperature anomalies observed during the ana-  
229 logue days. Figure 4 illustrates this approach for the year 2007 with analogues of circulation  
230 computed over the small domain. It shows that, for all observatories, the analogues reproduced  
231 the observed temperature anomalies quite well, but there was also a great variability between ana-  
232 logues. For certain days, the analogues could not capture the amplitude of the observed anomalies,  
233 as can be seen in the example from 17 to 20 January 2007 on all sites, February 2007 at SIRT  
234 and Cézeaux-COPDD, at the end of August 2007 at CRA-P2OA, and at the end of April 2007 at  
235 SIRT. A smaller standard deviation of the ten anomalies of analogous days combined with an av-  
236 erage closer to the temperature anomaly of the day in question means that the large scale explains

237 the anomaly. In our study, we investigated whether this departure from the observed series relative  
238 to the envelope defined by the atmospheric conditions on analogue days can be explained by local  
239 processes. Weather regimes were used to describe and better understand the large-scale influence  
240 (see indications of the regimes in Fig. 4).

### 241 **3. Analysis of large-scale conditions versus local processes**

242 In order to estimate the influence of the Mediterranean Sea relative to the Atlantic Ocean at the  
243 three sites, we first evaluated the ability of the analogues to represent the observed series using  
244 the two different domains described above. Afterward, the difference between the observed series  
245 and the temperature anomalies of the analogues was quantified by the definition and the use of  
246 an anomaly index. Finally, we focused on specific periods during which the difference was larger  
247 than 1.5 °C, tried to identify the relevant processes, and discussed the relative contribution of  
248 large-scale and local processes.

#### 249 *a. Sensitivity to the Mediterranean Sea*

250 Figure 5 presents the correlation between observed anomalies and those deduced from flow  
251 analogues in the large and small domains (Fig. 1b) for each site and for each season. All observed  
252 daily temperature anomalies for each season are correlated with those of their 10 analogue days.  
253 Thus, for each season of each year from 2003 to 2013, we have one correlation coefficient. This  
254 Figure points out larger correlation coefficients in the small domain than in the large domain. This  
255 is obvious for the two southern observatories whatever the season, whereas higher correlation  
256 coefficients across the small domain are observed only in summer and spring for SIRT A. This  
257 shows that SIRT A is more influenced by large-scale air masses coming from the Atlantic than by

258 mesoscale processes induced by orography and the presence of the Mediterranean Sea, which can  
259 strongly influence the weather across southern France (e.g Ducrocq et al. (2008)).

260 We found a large spatio-temporal variability in the correlation coefficients. CRA-P2OA indi-  
261 cated, on average, the lowest correlation coefficients for the two domains (0.52 and 0.35 respec-  
262 tively for the small and large domain) compared to the other two sites (for the small domain,  
263 Cézeaux-COPDD and SIRTA had respectively 0.55 and 0.57 and for the large domain, 0.38 and  
264 0.46 respectively). This difference can be due to the fact that CRA-P2OA is located in proximity  
265 to the Pyrenees, where local processes linked with topography exist: for example, local convec-  
266 tion or plain-mountain breeze circulations are more frequent in summer. The two cases of very  
267 low correlation with the large domain (at the bottom-left of each subplot in Fig. 5 with green and  
268 black colors) were observed in autumn 2011 at each site, during the winter of 2006 at SIRTA, and  
269 during the winter of 2008 at CRA-P2OA and Cézeaux-COPDD. The autumn of 2011 was excep-  
270 tionally warm. It was indeed the second warmest autumn during the period 1948-2011, after 2006,  
271 according to Cattiaux and Yiou (2012). Cattiaux and Yiou (2012) found that the flow analogues  
272 underestimated the amplitude of the seasonal temperature anomaly in Europe during this specific  
273 season. This suggests that global warming plays an important role by increasing the concentration  
274 of greenhouse gases: the advected air mass is warmer, but it can also enhance local feedbacks.

275 In the following section, we evaluate the flow analogues approach by considering only the  
276 smaller domain, in order to quantify the influence of local processes on the climate variability  
277 at the three sites.

### 278 *b. Large-scale influence*

279 We have attempted to better quantify the relative contribution of large scale versus local pro-  
280 cesses on the amplitude of temperature anomalies. Since the average signal of the analogues have

281 inherently lower magnitude fluctuations, we introduce  $I_m$ , a new normalized index to facilitate  
282 comparison of the observations and analogue series.

283 This index  $I_m$ , defined for each month  $m$ , represents the monthly average anomaly  $\langle aT(j) \rangle_m$   
284 relative to the standard deviation of the 2003-2013 daily anomalies for the given month  $m$ . We  
285 compute  $I_m$  with:

$$I_m = \frac{\langle aT(j) \rangle_m}{\sqrt{\langle (aT(j) - \langle aT(j) \rangle_{[m,2003-2013]})^2 \rangle_m}}, \quad (2)$$

286 where  $\langle aT(j) \rangle_{[m,2003-2013]}$  is the average anomaly of temperature of the current month  $m$  during  
287 the period 2003-2013. In other words, the red line in Fig. 4 is averaged monthly and divided by the  
288 standard deviation computed from the monthly anomalies for the period 2003-2013. Concerning  
289 the analogue signal, the same definition of the index is applied using all observed anomalies in the  
290 analogue days.

291 Figure 6 represents the time series of this index across the period 2003-2013. The flow analogues  
292 reproduce the variability of surface temperature anomalies particularly well. The correlation coef-  
293 ficients between  $I_m$  for observations and analogues are 0.80 for SIRTA, 0.85 for Cézeaux-COPDD  
294 and 0.86 for CRA-P2OA. This means that the large scale actually plays a predominant role in  
295 creating the temperature anomaly variability on monthly scales, which is not surprising.

296 In Fig. 6, one may note the spatio-temporal variability of  $I_m$  at the three observatories. The years  
297 2003 and 2011 were the warmest years at every site for the period 2003-2013, whereas the coldest  
298 year at every site was that of 2010 with negative  $I_m$  for every month.

299 While the general trend is well captured by  $I_m$  for analogue days, the magnitude of certain  
300 events is not reproduced. For example, February 2007 was exceptionally warm with  $I_m$  larger  
301 than 1.7 at SIRTA and Cézeaux-COPDD according to observations. This peak in temperature  
302 is not reproduced by flow analogues with an index of around 0.5 (Fig. 6) when using the small

303 domain, and is even negative when using the large domain (not shown). The large anomaly is not  
304 observed at CRA-P2OA. The spatial variability of temperature anomalies during this winter and  
305 the difference between observed anomalies and analogues allow us to hypothesize that specific  
306 synoptic-scale features leading to local anomalies that are not resolved by the analogue approach  
307 alone and that local processes may have played a specific role at each site during this period.

### 308 *c. Analysis of specific events during winter 2007*

309 We focused on the winter of 2006/2007 in order to further investigate the contribution of large  
310 and local-scale processes on the spatio-temporal variability of daily temperature anomalies at the  
311 observatories. Note that winter 2007 appears to be the warmest of our study period: it was the sec-  
312 ond warmest winter in France since 1959 according to climatology established by Meteo-France  
313 (<http://www.meteofrance.fr/>).

314 Figure 7 shows the time series of daily temperature anomalies for the winter of 2006/2007  
315 from observations and analogues. It focuses in on the period from January to February 2007 in  
316 Fig. 4. During this period, two regimes, “NAO+” and ”Atlantic ridge” are persistent. “NAO+” is  
317 associated with a southwesterly flow over Northern Europe (Michelangeli et al. 1995). We showed  
318 in section 2c that the two regimes, “NAO+” and “Atlantic Ridge” are usually the warmest in winter  
319 at all three sites. These results are consistent with those of Yiou et al. (2007) for the exceptionally  
320 warm 2006/2007 fall/winter. The regime  $NAO^-$  appears between 22 and 26 January, with negative  
321 anomalies at all sites. Snow was observed at SIRTA on 23 January, and from 23 to 25 January at  
322 CRA-P2OA and Cézeaux-COPDD.

323 We focused on specific warm events during the winter of 2007 to investigate the role of lo-  
324 cal processes on the spatio-temporal variability of daily temperature anomalies. We will further  
325 analyze two periods /dates: the period 17 to 19 January and a single day: 16 February 2007.

326 1) 17-19 JANUARY 2007 CASE

327 The period from 17 to 19 January encompasses the warmest anomalies of the month of January  
328 2007 at all sites (Fig. 7) with spatial variability in the amplitude: the southern site (CRA-P2OA)  
329 shows the lowest daily temperature anomalies compared to the other two sites (warmest anomaly  
330 of 9.4, 10 and 7.2 °C at SIRTA, Cézeaux-COPDD and CRA-P2OA respectively, on 18 January  
331 2007). The observed positive temperature anomalies are higher than those of analogue days for  
332 the whole 17-19 January period at SIRTA and Cézeaux-COPDD and only at CRA-P2OA for the 18  
333 January. Despite the spatial variability in the temperature anomalies, 18 January 2007 indicates an  
334 anomaly on a large scale and one can wonder why the anomaly's amplitude of such a large-scale  
335 event is not reproduced by any of the analogue days.

336 To answer this question, the large-scale meteorological situation of analogue days is verified  
337 using satellites and ERAI reanalyses and local effects are analyzed based on the meteorological  
338 history of the surface measurements and radiosoundings. The meteorological history provides a  
339 view of the atmospheric conditions of previous days on a local scale. We consider, therefore,  
340 the diurnal cycles on 18 January 2007 and on the two previous days (16 and 17 January 2007)  
341 to point out the effect of the “local meteorological history” at each site. Similarly, the “local  
342 meteorological history” of the five best analogue days on 18 January 2007 is presented. For  
343 example, if 20 December 2011 is one analogue day for 18 January 2007, the time series from 18  
344 to 20 December 2011 are displayed.

345 The large-scale circulation is the NAO<sup>+</sup> regime on 17 and 18 January, and “Atlantic ridge”  
346 on 19 January (Fig. 7). Figure 8 shows the wind speed and direction at 600 hPa from the ERAI  
347 reanalyses. It indicates an increasing westerly wind over France during the 16-18 January period.  
348 The five most accurate analogues are generally similar with an increasing wind speed from 17

349 to 18 January and show similar wind directions. On 16-17 January, only one analogue indicates  
350 similar wind speed and direction. However, wind speed varies from one analogue to another.

351 The reflectance in the visible channel at  $0.6 \mu\text{m}$  of the MeteoSat Second Generation (MSG) at  
352 1300 UTC on 18 January 2007 is shown in Fig. 9a. Significant cloud cover over the North Atlantic  
353 and Europe was observed with a window of clear sky over the Mediterranean basin, the South of  
354 Spain and the Pyrenees region. Similar cloud cover was also observed on 17 and 19 January  
355 2007 (not shown). The method of Wang and Rossow (1995) was applied to the vertical profile of  
356 relative humidity from the radiosoundings at Trappes on 18 January (Fig. 9b) to define the cloud  
357 base height. Wang and Rossow (1995) used among other criteria, 87% and 84% as maximum and  
358 minimum relative humidity thresholds respectively and relative humidity jumps exceeding 3% at  
359 cloud-layer top and base to characterize a cloud-layer. With this method, we find in Fig. 9b that  
360 on the 18 January, cloud cover was dominated by low-level clouds with a base not exceeding 700  
361 m in height at 1100 UTC. At 2300 UTC, cloud cover descended and thickened. Based on the  
362 Meteo-France weather service station, drizzle was observed that night, with 0.8 mm falling at this  
363 site. Combining the satellite image and vertical profiles of relative humidity, we find that these low  
364 clouds were stratocumulus clouds associated with the stable atmospheric conditions in Southern  
365 Europe linked to the NAO<sup>+</sup> regime. Indeed, the stratocumulus clouds occur widely over Europe  
366 in January, according to Hahn and Warren (2007). A similar analysis of the vertical profiles of  
367 relative humidity for the five most accurate analogue days (Fig. 9b) shows that 18 January 2007  
368 was the cloudiest day: either there was no cloud cover (analogue day number 3), or there was cloud  
369 cover which disappeared between 1100 and 2300 UTC (analogue day number 1), or much thinner  
370 cloud cover (analogue days number 4 and 5). We can expect an effect due to this cloud layer on  
371 18 January since it impacts the radiative budget at the surface at SIRTa and Cézeaux-COPDD.

372 The meteorological history of 18 January and its five most precise analogue days was analyzed  
373 with surface measurements. The large scale cloud cover, discussed previously (Fig. 9), impacts  
374 incoming solar radiation (ISR) (Fig. 10). The ISR measured at the surface increases from north  
375 to south, with very cloudy conditions at SIRTA for every day and almost no reduction of ISR  
376 at CRA-P2OA. The integration of ISR across the three days defining the meteorological history  
377 period (not shown) demonstrates low levels of ISR for the observed days compared to the analogue  
378 days at SIRTA and Cézeaux-COPDD, contrary to CRA-P2OA.

379 Figure 10 presents the time series of temperature, incoming shortwave radiation at 2 m, wind  
380 speed and direction at 10 m above the ground. Cloud cover also clearly impacts the diurnal cycle  
381 of 2m-temperature (Fig. 10); Low-level cloud cover at SIRTA reduces the cooling of the earth and  
382 damps the diurnal temperature cycle. This is also the case at Cézeaux-COPDD, on 18 January.  
383 On the contrary, a large diurnal temperature cycle can be observed at CRA-P2OA on most of the  
384 days, especially during the period 16-18 January.

385 At SIRTA, the westerly wind direction at the surface is consistent with the synoptic wind (Fig. 8).  
386 The wind direction at Cézeaux-COPDD is quite variable but maintains a westerly direction on av-  
387 erage, whereas a clear effect of the mountain range can be observed on 16, 17 and some of 18  
388 January at CRA-P2OA, with some north-easterly slope winds during the day and southerly at  
389 night, a sign of the plain-mountain diurnal circulation. Figure 10 shows the diversity of the con-  
390 ditions observed during the analogue days at CRA-P2OA, which makes the comparison difficult.  
391 Among the five most accurate analogue days, only three are cloud-free. All of them indicate a  
392 reversal of the wind direction twice a day. This is characteristic of the slope wind, which seems  
393 to play an important role and blurs the comparison of the diurnal cycle. During winter, a lack of  
394 cloud cover may allow weak convection over mountains, and certainly greater radiative cooling  
395 at night. This southerly mountain breeze during the night advects cool air from the mountains

396 and is associated with low temperatures at night. The mountain breeze which occurs during the  
397 NAO<sup>+</sup> regime could then reduce the positive temperature anomaly tendency associated with this  
398 regime. The meteorological history of 18 January shows a slope wind regime until noon, when a  
399 clear westerly wind settles at the surface. From that moment, the temperature clearly increases,  
400 and remains high during the night, with no mountain breezes, between 18 and 19 January. The  
401 daily mean temperature then leads to a larger positive temperature anomaly compared with the  
402 analogue days with slope winds lasting all day.

403 From these large and local-scale analyses of the observed days and their analogue days, we  
404 can ascribe this positive temperature anomaly to a large-scale event observed at the three sites.  
405 The NAO<sup>+</sup> regime, which advects mild temperatures from the Atlantic ocean, is characterized  
406 by the warmest temperature anomaly in winter (Fig. 3). The flow analogue method shows some  
407 limitations, however, in representing this event. The cloud layer is particularly low and deep,  
408 and lasts for three days over the northern part of France, whereas nothing in the meteorological  
409 history of the analogue days indicates such conditions. This cloud cover could imply a warming  
410 radiative effect over SIRT A and Cézeaux-COPDD during the 17-19 January period, which would  
411 amplify the positive anomaly due to what is already mild air advection. While the low cloud  
412 cover observed during this event is not a local effect, its radiative interaction with the surface is  
413 dependent on surface temperature and can be considered a local effect.

414 In conclusion, it seems that this abnormal warm event stands out from the analogue days, for  
415 various reasons at SIRT A and Cézeaux-COPDD in the first instance and then at CRA-P2OA.  
416 The large-scale positive anomaly associated with the NAO<sup>+</sup> regime is amplified at SIRT A and  
417 Cézeaux-COPDD by the warming radiative effect of an unusually low cloud cover occurring over  
418 the two sites during the 11 year period. This event, lasting for three days, lead to warmer anomalies  
419 than on analogue days. Meanwhile, in CRA-P2OA, the absence of clouds lead to a down-valley

420 wind regime which tends to cool the air at night and to reduce the NAO<sup>+</sup> regime warm anomaly.  
421 The down-valley wind was observed on 18 January until midday and did not occur the following  
422 night. This led to higher nocturnal temperatures and warmer daily temperature anomalies than on  
423 analogue days the following night. These results show that radiation and cloud cover are important  
424 predictors of daily temperature anomalies in winter at this observatory.

## 425 2) 16 FEBRUARY 2007 CASE

426 16 February 2007 is an example of a case where the temperature anomaly largely exceeded the  
427 range of the flow analogues at a single site. A strong and warm anomaly of 12.3 °C was observed  
428 at CRA-P2OA on that day, while all analogues showed an anomaly below 8 °C (Fig. 7). At the two  
429 other observatories, the temperature anomaly on this day was within the envelope of the analogues.

430 The synoptic atmospheric conditions on 16 February were forced by the presence of very low  
431 pressure centered over Iceland, and its associated thalweg extending from the island towards the  
432 south, near Spain and Morocco. This situation, which often announces the arrival of a front,  
433 generated a south-southwesterly wind regime in altitude, bringing dry and warm air from the  
434 south. The wind at 600 hPa across the three sites and deduced from the reanalyses of the European  
435 Center is shown in Fig. 11 for 16 February and for its analogous days. The analogues have the  
436 same types of southwesterly wind regime across the three sites. This situation generally leads to a  
437 positive temperature anomaly due to the southern origin of the air mass in many such cases. For  
438 this reason, on average, the envelope of the analogues shows a positive temperature anomaly at all  
439 sites (Fig. 7).

440 Southerly winds over the ridge of the Pyrenees correspond to the typical situation of the so-  
441 called foehn phenomenon: the east-west orientated mountain ridge is an obstacle for the flow,  
442 which can be partially blocked in the lower layers and which can bypass the ridge, with the flow

443 splitting at its sides, or/and passing over and through it across the mountain passes (Scorer 1949,  
444 1953, 1955; Scorer and Klieforth 1959; Seibert 1990; Ólafsson and Bougeault 1997; Jiang et al.  
445 2005). The adiabatic descent of air in the lee, usually occurring together with the flow over the  
446 mountain, is associated with a typical drying and warming in the lower lee air layers on the French  
447 side ('foehn effect').

448 One of the most important governing variables for this phenomenon is the upwind wind profile,  
449 and particularly the upwind component, which is perpendicular to the ridge: the larger this com-  
450 ponent, the easier it is for the flow to go over the mountain and generate the foehn effect (Seibert  
451 1990). For the Pyrenees in the vicinity of the CRA-P2OA site, we evaluate the cross-component  
452 at  $210^\circ$  azimuth ( $\pm 10^\circ$ ): that is, a wind with this direction (which is very similar to a southerly  
453 wind) travels exactly transversely to the ridge, on a 150 km horizontal scale. This direction is  
454 also aligned with the main Aure Valley, which is situated south of the CRA-P2OA observatory  
455 and North-South orientated. Figure 12a shows the upwind profiles of the cross-ridge component  
456 (projection of the wind on the  $210^\circ$  axis), for 16 February and for all analogues, at 0000 UTC.  
457 These are deduced from the radiosoundings launched daily from Zaragoza in Spain. Zaragoza is  
458 located about 150 km south of the ridge of the Pyrenees, and 200 km from the CRA-P2OA site.  
459 These profiles confirm the potential to generate the foehn effect at CRA-P2OA for most of the days  
460 shown, as this component is positive for most cases above 1000 m. It also reveals that 16 February  
461 is the case with the strongest  $210^\circ$  upwind component between 1000 m and 6000 m, especially  
462 below 3500 m, making it the most favorable case for a strong foehn event (the highest peak in the  
463 Pyrenees is at 3400 m). Figure 11 also shows a significant increased in wind speed upwind of the  
464 ridge during the day.

465 Figure 12b is a the visible image of MSG at 1500 UTC on 16 February 2007. This day was  
466 marked by large cloud cover over the western Atlantic and northern Europe, and a clear sky above

467 the Mediterranean basin and eastern Europe. Cloud cover over the Pyrenees shows that the sky  
468 was clear in Spain and in the lee of the mountain (where CRA-P2OA is situated). Farther to the  
469 north, a cloud with a well-defined southern border, typical of the upward branch of a mountain  
470 wave, can be observed, and is usually associated with foehn and southerly overpassing flows. The  
471 clear sky in Spain reveals a “dry foehn” as opposed to some cases, where clouds are blocked on  
472 the Spanish side, with some rain that can contribute to the drying and warming effect of the air in  
473 the lee on the French side. This means that on 16 February, air mass was generally very dry at the  
474 large scale, a fact which is confirmed by the radiosoundings taken at Zaragoza, Bordeaux (Atlantic  
475 French coast), Trappes (close to Paris), and the synoptic situation discussed before. The Trappes  
476 soundings at 1100 and 2300 UTC show very dry and warm air between 800 m and 4000 m. Above  
477 this altitude, fine medium clouds (of about 500 m) are observed (not shown).

478 We can now consider the observations at the surface of the different observatories. Figure 13  
479 presents the evolution of the meteorological variables observed close to the surface on 16 February  
480 2007, and its analogues. The most striking feature is found in the surface wind at CRA-P2OA: for  
481 all the analogues, the wind at the surface is southerly during the night and northerly during the day.  
482 This, along with the low associated wind speed (below  $6 \text{ m s}^{-1}$ ), is indicative of the mountain-plain  
483 diurnal circulation. That is to say, although the upwind flow is from the south, and sometimes has  
484 a strong wind speed (Fig. 12a), this does not prevent the plain-mountain circulation from setting  
485 up during those analogue days. It is actually quite classic, with the southerly wind kept at a higher  
486 level. Note that this does not prevent the foehn effect (warming and drying in the lee), or the  
487 warmer local temperature that can be found at this site relative to the other sites. On 16 February,  
488 however, the wind at the surface of CRA-P2OA remained southerly all day, with the wind speed  
489 increasing during the day, by up to  $10 \text{ m s}^{-1}$  at times. This means that for this specific day, the  
490 upwind flow was strong enough to be able to create a downslope wind throughout the entire day in

491 which case, the warming and drying effect in the lee is still larger. This is consistent with Fig. 12a,  
492 which shows the characteristics of this day in terms of upwind conditions. It probably explains  
493 most of the temperature anomalies found at CRA-P2OA, which exceed the usual anomalies found  
494 in analogous synoptic situations (Fig. 7).

495 At Cézeaux-COPDD, this synoptic situation does not lead to a marked anomaly, but the general  
496 dry and warm air leads to a large diurnal increase. The night of 16 to 17 February may have been  
497 influenced by a small foehn effect, in the presence of westerly winds (typically occurring in the  
498 “Chaine des puys” mountains to the west of the site). The air temperature does not decrease  
499 much, and the wind continues to arrive from the west. At SIRTA, the wind at the surface is  
500 easterly, surprisingly, while the sounding at Trappes shows a strong southerly flow down to the  
501 lowest levels of the atmosphere. This weak easterly wind at SIRTA seems unconnected to the  
502 warm, dry southerly air above, and could explain the relative lower temperature found on 16  
503 February (relative to its analogues).

504 This event shows how meso- $\beta$  scale processes linked with orography can amplify a temperature  
505 anomaly which is primarily forced at the synoptic scale. This specific type of amplification has  
506 been previously observed by Takane and Kusaka (2011) in Japan in the summer.

#### 507 **4. Summary and Conclusions**

508 This study aimed to evaluate the relative contribution of large-scale atmospheric circulation and  
509 more local processes to daily temperature anomalies over a north-south transect of France. The  
510 study was based on the observations of meteorological variables at three observatories and on  
511 NCEP and ECMWF reanalyses. The flow analogues method was used in particular to diagnose  
512 the fingerprint of the large-scale synoptic circulations concerning the temperature anomaly, and to  
513 highlight the potential role of local processes in inhibiting or amplifying the anomaly.

514 The analysis of weather regimes over the Euro-Atlantic region shows that the large-scale atmo-  
515 spheric circulations have an important influence on the daily temperature anomalies at the three  
516 observatories in winter. The “NAO<sup>+</sup>” and “Atlantic Ridge” appear to be the warmest regimes in  
517 this season. While the influence of the four weather regimes on daily temperature anomalies does  
518 not statistically differ at the three observatories in the summer due to strong variability within each  
519 regime, extreme anomalies are associated with one or two regimes at all observatories except for  
520 that of SIRT A.

521 The flow analogue approach applied over two different domains shows that SIRT A is less af-  
522 fected by the mesoscale processes formed around the Mediterranean Sea than the other two obser-  
523 vatories, which is not surprising considering its northern location.

524 The atmospheric circulation analogue method demonstrates the large correlation between a  
525 monthly temperature anomaly index calculated from the observed series and that which is pro-  
526 vided by the representation of the analogues. This highlights the predominant role played by the  
527 large-scale situation in the temperature anomalies. Sometimes, however, the amplitude of the  
528 monthly temperature index is not captured by the flow analogues and shows a large spatial vari-  
529 ability between the three observatories. It is suggested that these discrepancies are related to local  
530 processes. Two specific events revealed in the warmest winter in the period 2003-2013 are further  
531 analyzed to test this hypothesis: 1) the 17-19 January 2007 event which had the strongest posi-  
532 tive temperature anomaly at the two northern observatories (SIRT A and Cézeaux-COPDD) and,  
533 2) the 16 February 2007, for which only CRA-P2OA indicated a very large positive temperature  
534 anomaly, found beyond the signal of the set of analogues.

535 From the analysis of these two events, the impact of several local processes have been identified:

536 1) the local impact of non-local cloud cover during westerly wind conditions in winter: low-level  
537 clouds have been shown to increase the positive temperature anomaly at SIRTA and Cézeaux-  
538 COPDD in these conditions, partly due to the positive radiative green-house effect of the clouds.

539 2) the orographic impact: CRA-P2OA and Cézeaux-COPDD are both in proximity to mountains  
540 and are frequently impacted by either foehns or slope wind effects. In a weak large-scale situation,  
541 the slope breeze easily settles at CRA-P2OA, and can transport cool air from the mountains during  
542 the night in winter. Foehn events observed at both the CRA-P2OA and Cézeaux-COPDD sites with  
543 southerly and westerly wind conditions respectively, can amplify positive temperature anomalies,  
544 originally forced by large scales.

545 The analysis of two specific events reveals that some local processes are able to modulate the  
546 trend of the daily temperature anomaly driven by the large-scale atmospheric circulation. How-  
547 ever, such a phenomenological approach remains difficult, since the understanding of one event  
548 necessitates the analysis of the meteorological history of not only the event itself, but also of its  
549 analogue days. To investigate the impact of local processes, a systematic study of all cases in  
550 which observations differ from analogue days would be necessary.

551 Departures between observed local anomalies and analogues might not only be due to local  
552 processes but also to differences between the observed event and its analogues on the synoptic  
553 scale, which would not be adequately resolved by the classical analogue approach employed. A  
554 possibility for the investigation of this is the combining of different variables in the analogues  
555 method (vorticity, water vapor, temperature, wind). Even if this would require much longer series  
556 in order to ensure a large enough number of analogues for each day.

557 *Acknowledgments.* This work was carried out in the context of ROSEA, and funded by AL-  
558 LENVI. The ROSEA program now belongs to a larger program and national network called AT-

559 MOS (Atmospheric Short-Lived Climate Forcers Observing System). The administrative and  
560 technical supervision of the observatories have been acknowledged. Part of the data used here  
561 were collected at the Pyrenean Platform for Observation of the Atmosphere P2OA, Observa-  
562 toire de Physique du Globe de Clermont Ferrand OPGC and Site Instrumental de Recherche par  
563 Télédétection Atmosphérique SIRTA. P2OA facilities and staff were funded and supported by the  
564 Observatoire Midi-Pyrénées (University of Toulouse, France) and the CNRS (Centre National de  
565 la Recherche Scientifique) INSU (Institut National des Sciences de l'Univers). OPGC facilities  
566 and staff were funded and supported by the Blaise Pascal University of Clermont Ferrand and  
567 CNRS (Centre National de la Recherche Scientifique) INSU. We are grateful to NCEP, ECMWF,  
568 and Meteo-France for providing the observation data and global model reanalyses used in this  
569 study. We acknowledge the CNES for partially funding M. Chiriaco's research. P. Yiou was sup-  
570 ported by an ERC advanced grant (No. 338965 - A2C2 ). The authors would like to thank the three  
571 anonymous reviewers for their fruitful comments, which helped us to improve the manuscript. Fi-  
572 nally, we thank Naomi RIVIERE and Eric PARDYJAK for carefully proof reading our manuscript.

## 573 **References**

- 574 Bastin, S., M. Chiriaco, and P. Drobinski, 2016: Control of radiation and evaporation on tem-  
575 perature variability in a wrf regional climate simulation: comparison with colocated long term  
576 ground based observations near paris. *Climate Dyn.*, doi:10.1007/s00382-016-2974-1.
- 577 Boé, J., and L. J. Terray, 2014: Land-sea contrast, soil-atmosphere interactions and cloud-  
578 temperature interactions: interplays and roles in future summer european climate change. *Cli-*  
579 *mate Dyn.*, **42(3-4)**, 683–699.

- 580 Cassou, C., L. Terray, and A. S. Phillips, 2005: Tropical atlantic influence on european heat waves.  
581 *J. Climate*, **18**, 2805–2811.
- 582 Cattiaux, J., R. Vautard, C. Cassou, P. Yiou, V. Masson-Delmotte, and F. Codron, 2010: Winter  
583 2010 in europe: A cold extreme in a warming climate. *Geophys. Res. Lett.*, **37**, doi:10.1029/  
584 2010GL044613.
- 585 Cattiaux, J., and P. Yiou, 2012: Contribution of atmospheric circulation to remarkable European  
586 temperatures of 2011, in Explaining Extreme Events of 2011 from a Climate perspective . *Bull.*  
587 *Amer. Meteor. Soc.*, **93**, 1041–1067, doi:10.1175/BAMSD-12-00021.1.
- 588 Cheng, X. H., and J. M. Wallace, 1993: Cluster analysis of the northern hemisphere wintertime 50  
589 hpa height field: Spatial patterns. *J. Atmos. Sci.*, **50(16)**, 2674–2696.
- 590 Cheruy, F., J. L. Dufresne, F. Hourdin, and A. Ducharne, 2014: Role of clouds and land-  
591 atmosphere coupling in midlatitude continental summer warm biases and climate change am-  
592 plification in cmip5 simulations. *Geophys. Res. Lett.*, **41**, 6493–6500.
- 593 Cheruy, F., J. C. Dupont, A. Campoy, A. Ducharne, F. Hourdin, M. Haeffelin, and M. Chiri-  
594 aco, 2013: Combined influence of atmospheric physics and soil hydrology on the realism  
595 of the lmdz model compared to sirta measurements. *Climate Dyn.*, **40**, 2251–2269, doi:  
596 10.1007/s00382-012-1469-y.
- 597 Chiriaco, M., S. Bastin, P. Yiou, M. Haeffelin, J. C. Dupont, and M. Stéfanon, 2014: European  
598 heatwave in july 2006: Observations and modeling showing how local processes amplity cin-  
599 ducive large-scale conditions. *Geophys. Res. Lett.*, **41**, doi:10.1002/2014GL060205.
- 600 Dee, D. P., and Coauthors, 2011: The era-interim reanalysis: configuration and performance of the  
601 data assimilation system. *Quart. J. Roy. Meteor. Soc.*, **137**, 553–597, doi:DOI:10.1002/qj.828.

- 602 Ducrocq, V., O. Nuissier, D. Ricard, C. Lebeaupin, and T. Thouvenin, 2008: A numerical study  
603 of three catastrophic precipitating events over southern france. part ii: Mesoscale triggering and  
604 stationarity factors. *Quart. J. Roy. Meteor. Soc.*, **134**, 131–145.
- 605 Fischer, E. M., S. I. Seneviratne, D. Lüthi, and C. Schär, 2007b: The contribution of land-  
606 atmosphere coupling to recent european summer heatwaves. *Geophys. Res. Lett.*, **34**, L06707,  
607 doi:10.1029/2006GL029068.
- 608 Haeffelin, e. a., M., 2005: Sirta, a ground-based atmospheric observatory for cloud and aerosol  
609 research. *Ann. Geophys.*, **23**, 253–275.
- 610 Hahn, C. J., and S. G. Warren, 2007: A gridded climatology of clouds over land (1971-96)  
611 and ocean (1954-97) from surface observations worldwide. Numeric data package ndp-026e  
612 ornl/cdiac-153, cdiac, Department of Energy. doi:10.3334/CDIAC/cli.ndp026e.
- 613 Jiang, Q., J. D. Doyle, and R. B. Smith, 2005: Blocking, descent and gravity waves: Observations  
614 and modeling of a map northerly föhn event. *Quart. J. Roy. Meteor. Soc.*, **131**, 675–701.
- 615 Kalnay, e. a., E., 1996: The ncep/ncar 40-year reanalysis project. *Bull. Amer. Meteor. Soc.*, **77**,  
616 437–471.
- 617 Lorenz, E. N., 1969: Atmospheric predictability as revealed by naturally occurring analogues. *J.*  
618 *Atmos. Sci.*, **26**, 636–646.
- 619 Luterbacher, J., and Coauthors, 2007: Exceptional european warmth of autumn 2006 and winter  
620 2007: Historical context, the underlying dynamics, and its phenological impacts. *Geophys. Res.*  
621 *Lett.*, **34**, L12704, doi:10.1029/2007GL029951.
- 622 Michelangeli, P. A., R. Vautard, and B. Legras, 1995: Weather regimes: Recurrence and quasi  
623 stationarity. *J. Atmos. Sci.*, **52**, 1237–1256.

624 Miralles, D. G., A. J. Teuling, C. C. V. Heerwaarden, and J. V. G. de Arellano, 2014: Mega-  
625 heatwave temperatures due to combined soil desiccation and atmospheric heat accumulation.  
626 *Nature Geosci.*, **7**, 345–349.

627 Ólafsson, H., and P. Bougeault, 1997: The effect of rotation and surface friction on orographic  
628 drag. *J. Atmos. Sci.*, **54**, 193–210.

629 Quesada, B., R. Vautard, P. Yiou, M. Hirschi, , and S. I. Seneviratne, 2012: Asymmetric european  
630 summer heat predictability from wet and dry southern winters and springs. *Nature Climate*  
631 *Change.*, **2**, 736–741, doi:10.1038/nclimate1536.

632 Schär, C., P. L. Vidale, D. Luthi, C. Frei, C. Haberli, M. A. Linigier, and C. Appenzeller, 2004:  
633 The role of increasing temperature variability in european summer heatwaves. *Nature*, **427**,  
634 332–336.

635 Scorer, R. S. I., 1949: Theory of waves in the lee of mountains. *Quart. J. Roy. Meteor. Soc.*, **75**,  
636 41–56.

637 Scorer, R. S. I., 1953: Theory of mountain waves: Ii - The flow over ridge. *Quart. J. Roy. Meteor.*  
638 *Soc.*, **79**, 70–83.

639 Scorer, R. S. I., 1955: Theory of mountain waves: Iv - separation of flow from the surface. *Quart.*  
640 *J. Roy. Meteor. Soc.*, **81**, 340–350.

641 Scorer, R. S. I., and H. Klieforth, 1959: Theory of mountain waves of large amplitude. *Quart. J.*  
642 *Roy. Meteor. Soc.*, **85**, 131–143.

643 Seibert, P., 1990: South foehn studies since the alpeX experiment. *Meteor. Atmos. Phys.*, **43**, 91–  
644 103.

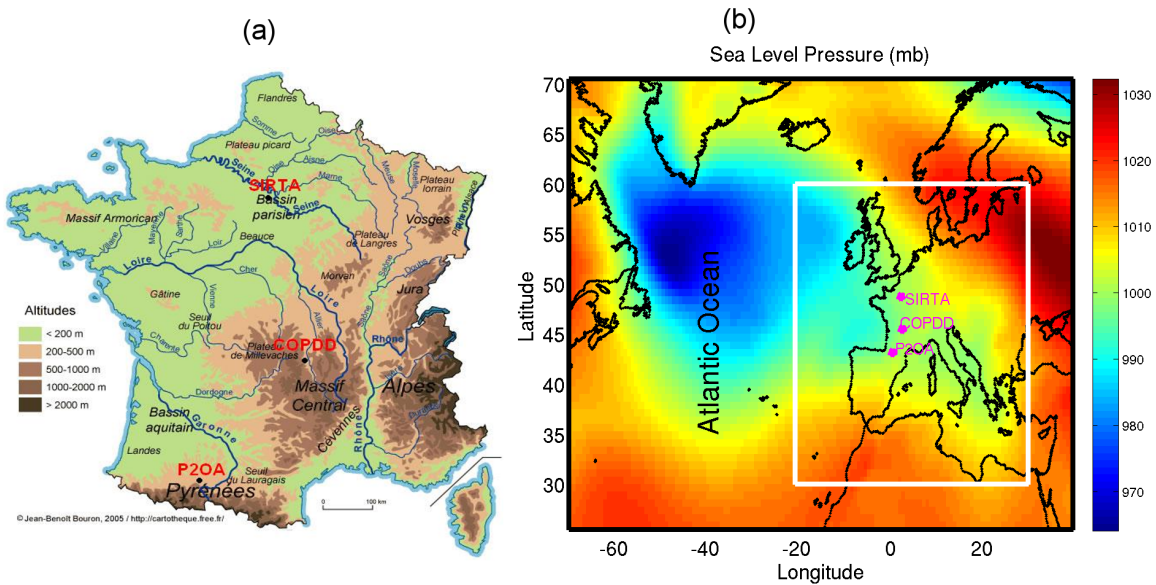
- 645 Seneviratne, S. I., D. Lüthi, M. Litschi, and C. Schär, 2006: Land-atmosphere coupling and climate  
646 change in europe. *Nature*, **443**, 205–209.
- 647 Seneviratne, S. I., P. Viterbo, D. Lüthi, and C. Schär, 2004: Inferring changes in terrestrial water  
648 storage using era-40 re-analysis data: The mississippi river basin. *J. Climate*, **17**, 2039–2057.
- 649 Stefanon, M., P. Drobinski, F. D’Andrea, C. Lebeaupin-Brossier, and S. Bastin, 2014: Soil  
650 moisture-temperature feedbacks at meso-scale during summer heat waves over western europe.  
651 *Climate Dyn.*, **42(4-5)**, 1309–1324, doi:0.1007/s00382-013-1794-9.
- 652 Stegehuis, A. I., A. J. Teuling, P. Ciais, R. Vautard, and M. Jung, 2013: Future european tempera-  
653 ture change uncertainties reduced by using land heat flux observations. *Geophys. Res. Lett.*, **40**,  
654 2242–2245, doi:10.1002/grl.50404.
- 655 Takane, Y., and H. Kusaka, 2011: Formation mechanisms of the extreme high surface air temper-  
656 ature of 40.9°c observed in the tokyo metropolitan area: Considerations of dynamic foehn and  
657 foehnlike wind. *J. Appl. Meteor. Climatol.*, **50**, 1827–1841.
- 658 Van den Dool, H., 2007: *Empirical Methods in Short-Term Climate Prediction*. Oxford University  
659 press.
- 660 Vautard, R., and P. Yiou, 2009: Control of recent european surface climate by atmospheric flow.  
661 *Geophys. Res. Lett.*, **36**, L22702, doi:10.1029/2009GL040480.
- 662 Vautard, R., and Coauthors, 2007: Summertime european heat and drought waves induced  
663 by wintertime mediterranean rainfall deficit. *Geophys. Res. Lett.*, **34**, L07711, doi:10.1029/  
664 2006GL028001.
- 665 Vrac, M., P. V. Ayar, and A. Yiou, 2013: Trends and variability of seasonal weather regimes. *Int.*  
666 *J. Climatol.*, **34**, 472–480, doi:10.1002/joc.3700.

- 667 Wang, J. H., and W. B. Rossow, 1995: Determination of cloud structure from upper-air observa-  
668 tions. *J. Appl. Meteor.*, **34**, 2243–2258.
- 669 Yiou, P., K. Goubanova, X. Z. Li, and M. Nogal, 2008: Weather regime dependence of extreme  
670 value statistics for summer temperature and precipitation. *Nonlin. Processes. Geophys.*, **15**,  
671 365–378, doi:10.5194/npg-15-365-2008.
- 672 Yiou, P., and M. Nogaj, 2004: Extreme climatic events and weather regimes over the north atlantic:  
673 When and where? *Geophys. Res. Lett.*, **31**, L07202, doi:10.1029/2003/GL019119.
- 674 Yiou, P., R. Vautard, P. Naveau, and C. Cassou, 2007: Inconsistency between atmospheric dy-  
675 namics and temperatures during the exceptional 2006/2007 fall/winter and recent warming in  
676 europe. *Geophys. Res. Lett.*, **34**, L21808, doi:10.1029/2007GL031981.
- 677 Zampieri, M., F. D’Andrea, R. Vautard, P. Ciais, N. de Noblet-Ducoudr, and P. Yiou, 2009: Hot  
678 european summers and the role of soil moisture in the propagation of the mediterranean drought.  
679 *J. Climate*, **22**, 4747–4758.

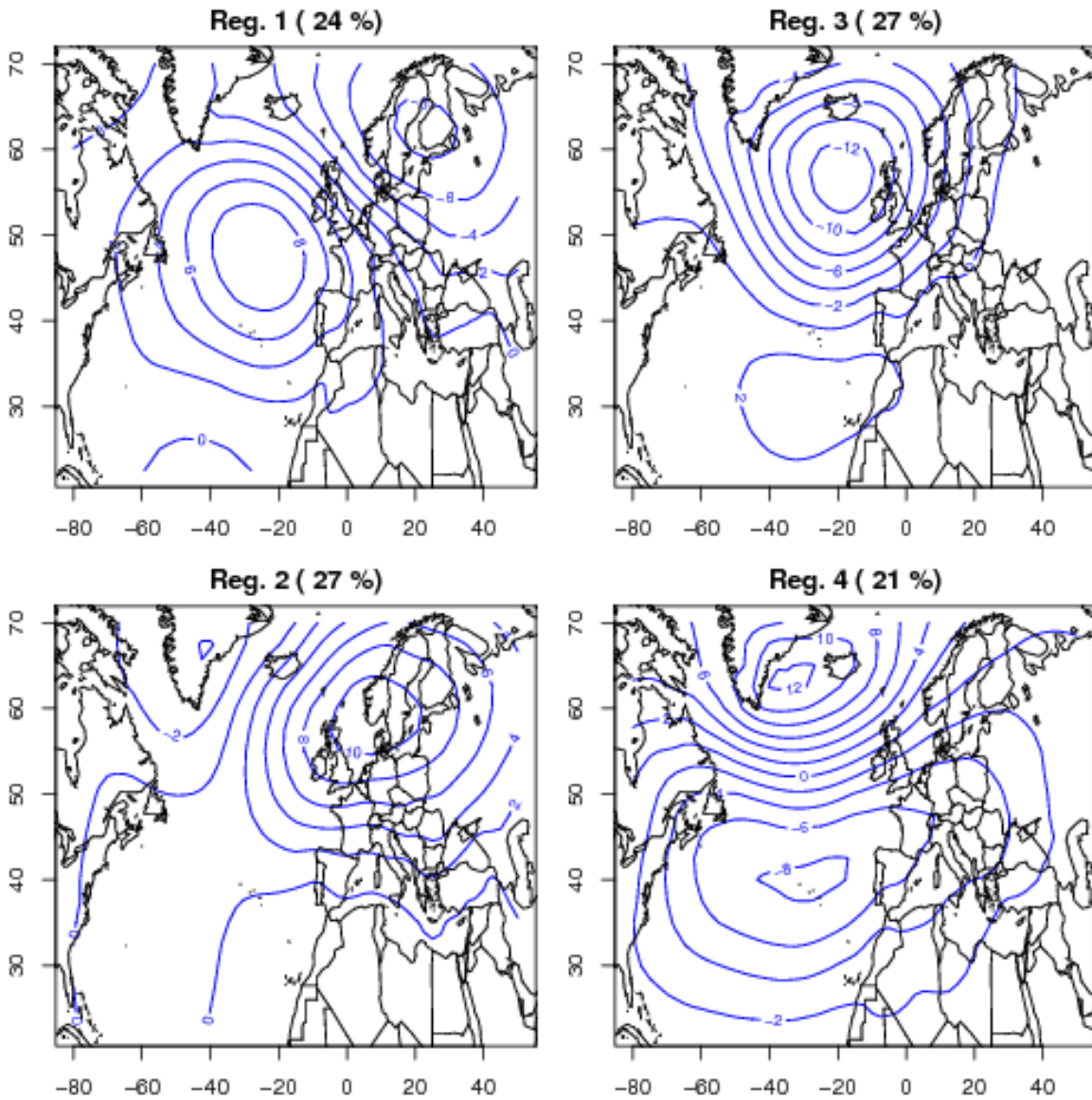
## LIST OF FIGURES

680		
681	<b>Fig. 1.</b>	(a) Orography of France and the locations of the SIRTA, COPDD and P2OA observatories (adapted from <a href="http://carthoteque.free.fr">http://carthoteque.free.fr</a> ). (b) Sea level pressure on 1 January 2003 from NCEP over the Euro-Atlantic domain used to define weather regimes and flow analogues in the large domain. The white square delimits the small domain used in the flow analogue method (see section 2). . . . . 34
682		
683		
684		
685		
686	<b>Fig. 2.</b>	Occurrence of North Atlantic weather regimes computed from the SLP from NCEP reanalyses in winter during the period 1948-2014. The frequency of each regime is in percentages at the top of each picture. Reg. refers to the weather regime and Reg. 1 is “Atlantic Ridge”, Reg. 2 is the “blocking”, Reg. 3 is NAO <sup>+</sup> , and Reg. 4 is NAO <sup>-</sup> . The isolines indicate the SLP anomalies in hPa. . . . . 35
687		
688		
689		
690		
691	<b>Fig. 3.</b>	Box plots of daily temperature anomalies for each weather regime during the period 2003-2013 at the three sites of the ROSEA network. . . . . 36
692		
693	<b>Fig. 4.</b>	Time series of daily temperature anomalies observed in 2007, (red) on current days and (gray) on analogue days at (a-d) SIRTA, (b-e) Cézeaux-COPDD and (c-f) CRA-P2OA. Colored bands at the top of each picture indicate the weather regime observed for each day: (blue) “NAO <sup>+</sup> ” (black) “NAO <sup>-</sup> ” (cyan) “Atlantic Ridge” and (red) “Blocking”. The gray envelope delimits the extreme values of the daily temperature anomalies from the set of analogue days. “an2” indicates the temperature anomalies of the analogue days computed in the small domain. Vertical blue dashed lines indicate the 17-20 January 2007 period. . . . . 37
694		
695		
696		
697		
698		
699		
700	<b>Fig. 5.</b>	Scatter plots of seasonal correlation coefficients between the large and small domain. The correlation coefficients are computed between observed and all analogue day temperature anomalies. Each color represents one season: winter (December-February) in black, spring (March to May) in blue, summer (June to August) in red and autumn (September to November) in green. The black cross indicates the winter of 2007. . . . . 38
701		
702		
703		
704		
705	<b>Fig. 6.</b>	Time series of the monthly normalized index of temperature anomalies observed (red line) and deduced from flow-analogues of the small domain (black line). The vertical dashed lines delimit the four seasons of the year (DJF, MAM, JJA, and SON). . . . . 39
706		
707		
708	<b>Fig. 7.</b>	As in Fig. 4, but zoomed in on January-February 2007. Horizontal black segments indicate the two specific events analyzed in sections 3.c.1) and 3.c.2). Colored squares at the top of each picture indicate the weather regime observed for each day: (blue) “NAO <sup>+</sup> ” (black) “NAO <sup>-</sup> ” (cyan) “Atlantic Ridge” and (red) “Blocking”. . . . . 40
709		
710		
711		
712	<b>Fig. 8.</b>	Time series at each site of wind speed and direction for the period from 16 to 18 January 2007 at 600 mb. The observed series are represented in “black” while the other colors represent the five most accurate analogue days for 18 January 2007. . . . . 41
713		
714		
715	<b>Fig. 9.</b>	(a) Reflectance in the visible channel of MSG/SEVIRI at 0.6 $\mu m$ on 18 January 2007 at 1300 UTC. This image is available at <a href="http://www.icare.univ-lille1.fr">http://www.icare.univ-lille1.fr</a> . Red points in (a) indicate the location of the three observatories. (b) Vertical profile of relative humidity at SIRTA at 1100 and 2300 UTC, respectively, on 18 January 2007. Solid lines indicate the observed vertical profiles, while dashed lines represent the five most accurate analogues. Vertical dashed lines in (b) indicate the minimum (84%) and maximum (87%) relative humidity used by Wang and Rossow (1995) to estimate cloud vertical structure: cloud-top and cloud-base heights. No radiosoundings at 2300 UTC for the analogue days number 2 and 3. . . . . 42
716		
717		
718		
719		
720		
721		
722		

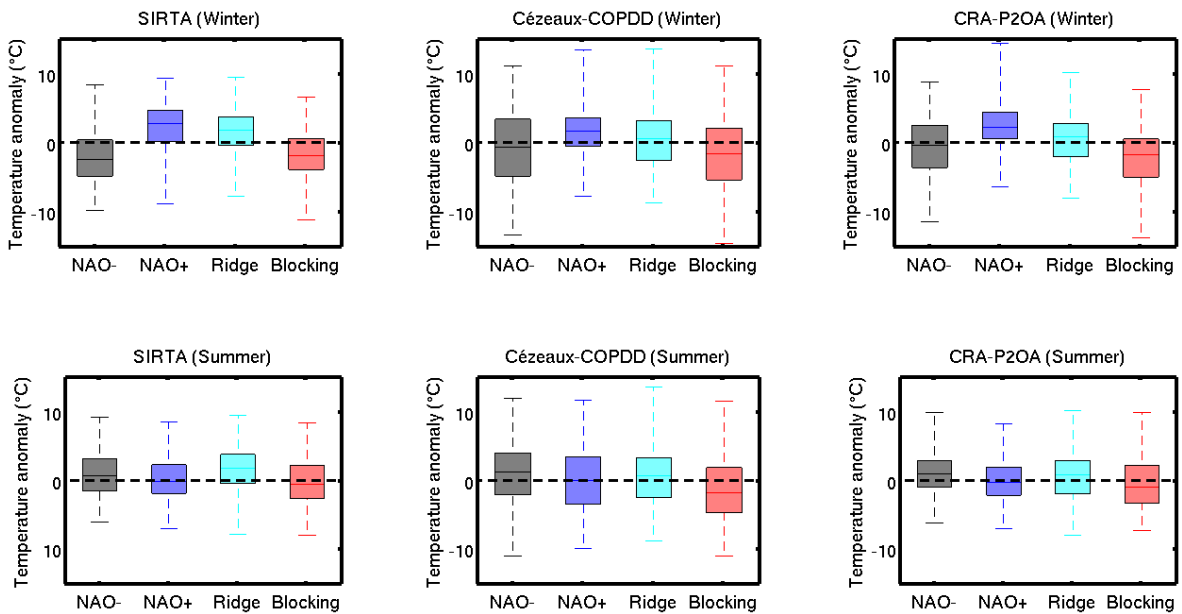
723	<b>Fig. 10.</b> Time series at each site of the temperature, incoming shortwave radiation (ISR), wind speed	
724	and direction during the period 16 to 18 January 2007. The observed series are represented	
725	in “black”, while the other colors represent the historical data of the five most accurate	
726	analogue days for 18 January 2007. . . . .	43
727	<b>Fig. 11.</b> As in Fig. 8 but for 16 February. . . . .	44
728	<b>Fig. 12.</b> (a) Reflectance in the visible channel of MSG/SEVIRI at $0.6 \mu m$ on 16 February 2007 at	
729	1500 UTC. This image is available at the following site: <a href="http://www.icare.univ-lille1.fr">http://www.icare.univ-lille1.fr</a> . Red	
730	points in (b) indicate the location of the three observatories; the blue point represents the	
731	radiosonde station in Zaragoza. (b) Vertical profiles of the cross wind component to the	
732	Pyrenees ridge ( $210^\circ$ ) observed at Zaragoza, Spain, on 16 February and the entirety of its	
733	analogues, at 0000 UTC, . . . . .	45
734	<b>Fig. 13.</b> As in Fig. 10 but for 16 February. . . . .	46



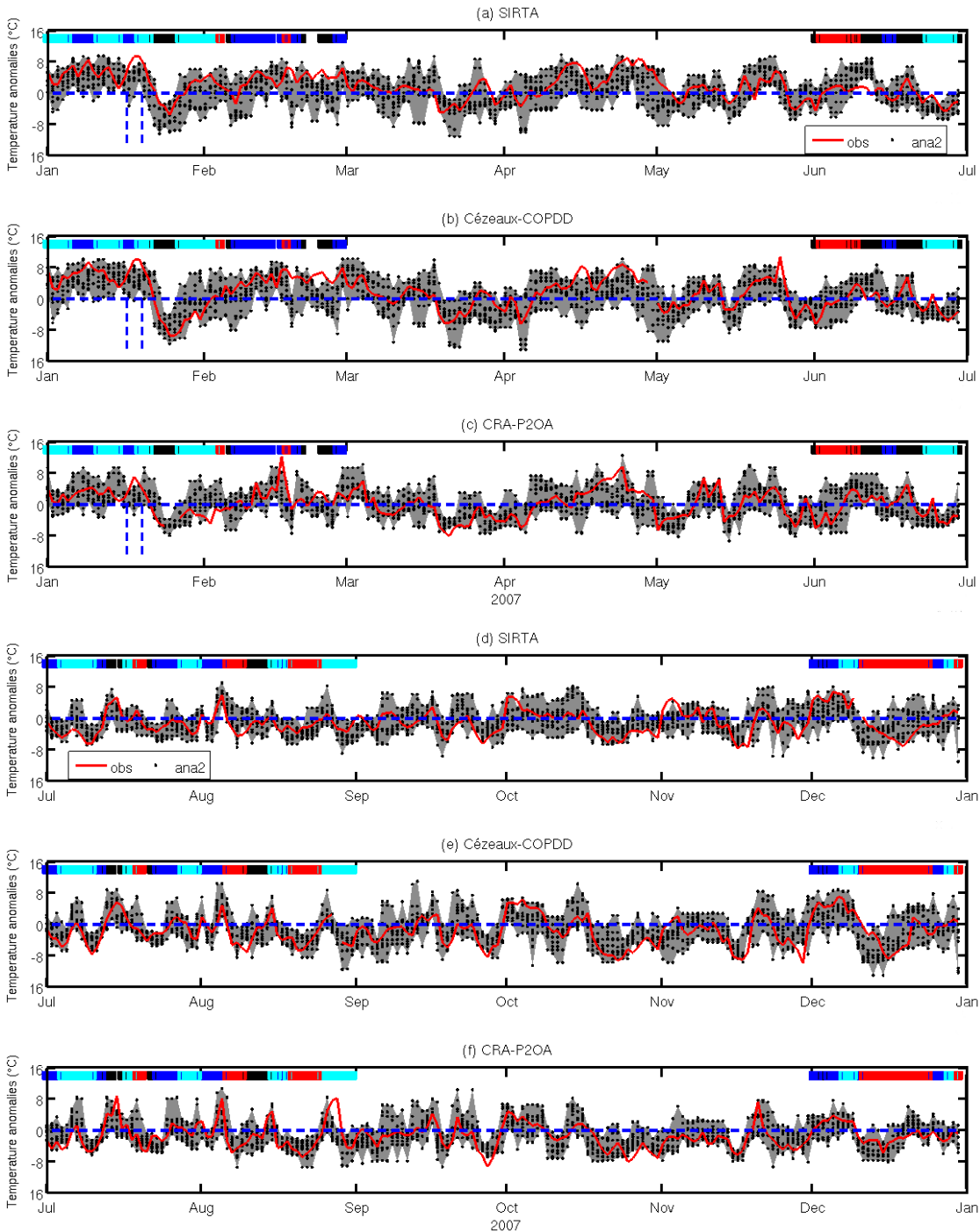
735 FIG. 1. (a) Orography of France and the locations of the Sirta, COPDD and P2OA observatories (adapted  
 736 from <http://carthoteque.free.fr>). (b) Sea level pressure on 1 January 2003 from NCEP over the Euro-Atlantic  
 737 domain used to define weather regimes and flow analogues in the large domain. The white square delimits the  
 738 small domain used in the flow analogue method (see section 2).



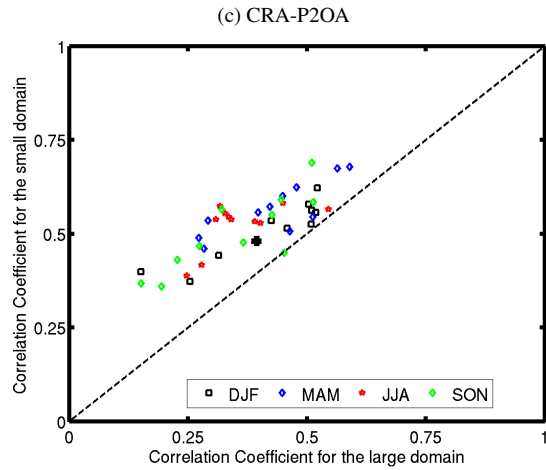
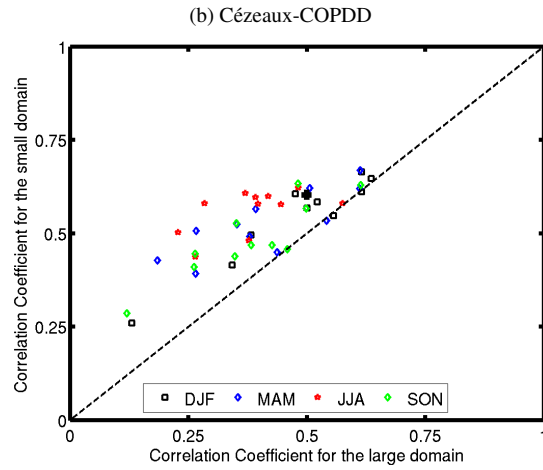
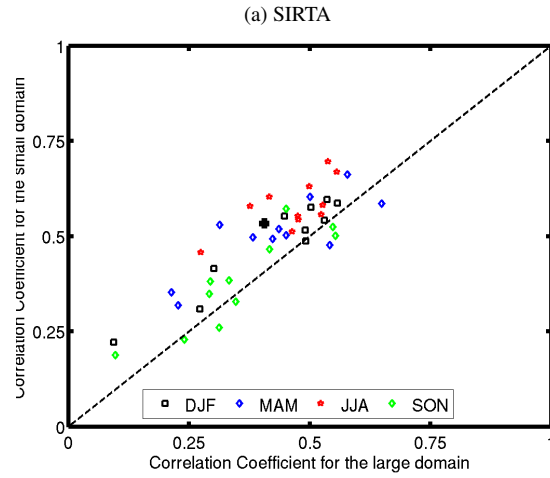
739 FIG. 2. Occurrence of North Atlantic weather regimes computed from the SLP from NCEP reanalyses in  
 740 winter during the period 1948-2014. The frequency of each regime is in percentages at the top of each  
 741 picture. Reg. refers to the weather regime and Reg. 1 is “Atlantic Ridge”, Reg. 2 is the “blocking”, Reg. 3 is  
 742  $NAO^+$ , and Reg. 4 is  $NAO^-$ . The isolines indicate the SLP anomalies in hPa.



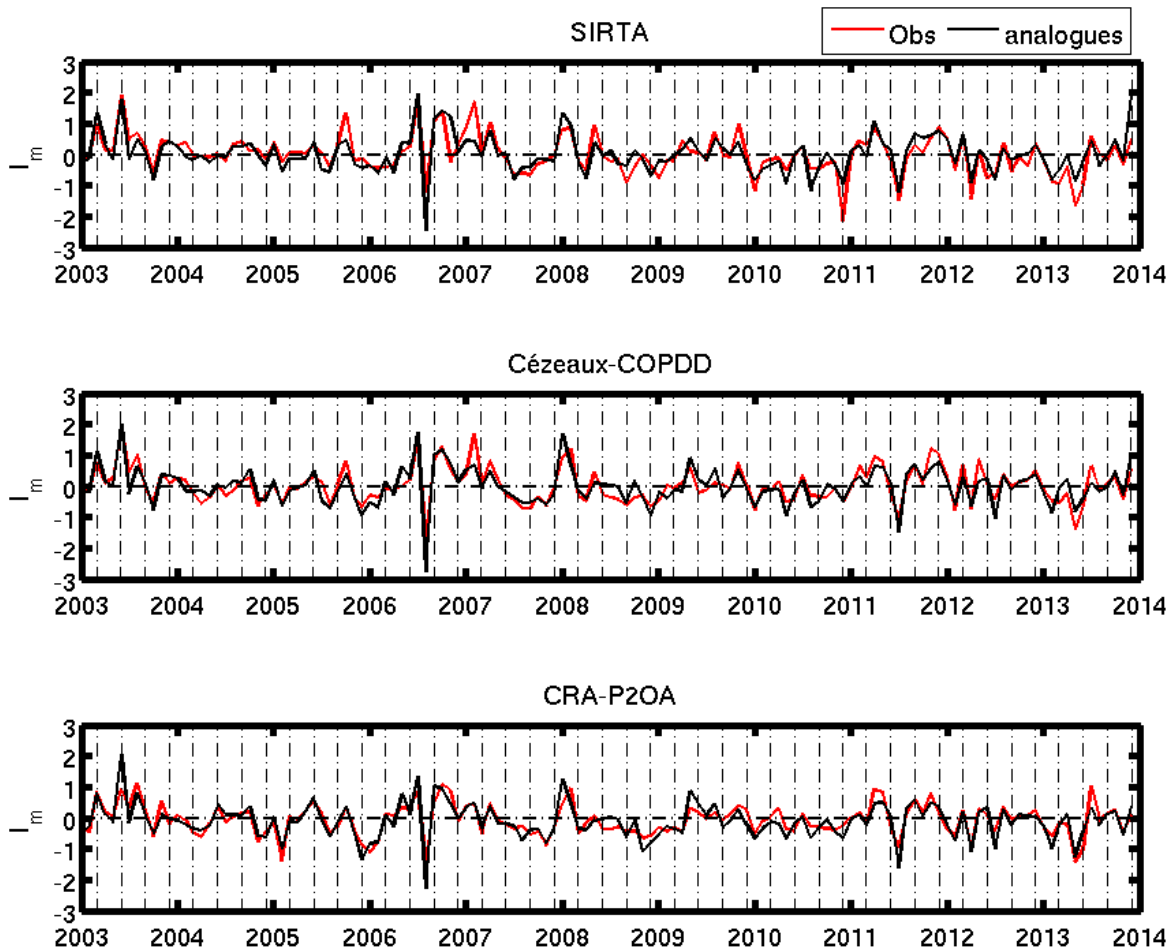
743 FIG. 3. Box plots of daily temperature anomalies for each weather regime during the period 2003-2013 at the  
 744 three sites of the ROSEA network.



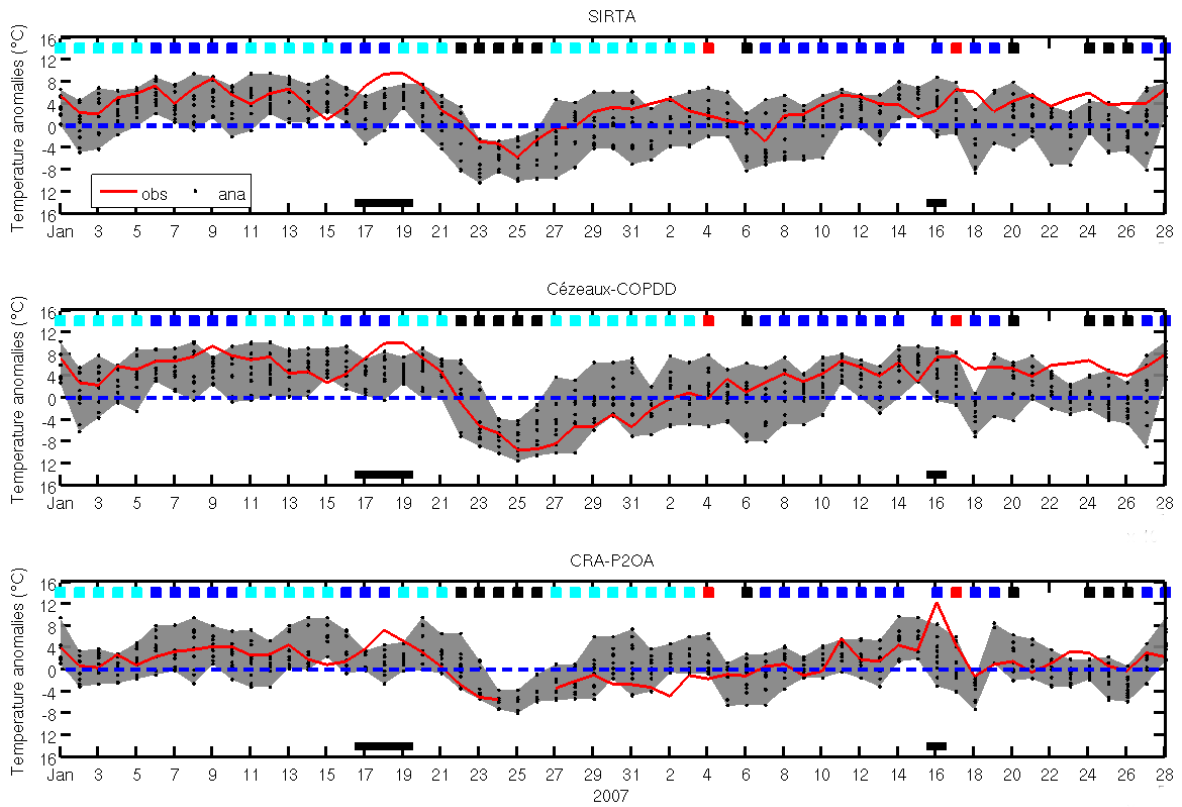
745 FIG. 4. Time series of daily temperature anomalies observed in 2007, (red) on current days and (gray) on  
 746 analogue days at (a-d) SIRTA, (b-e) Cézeaux-COPDD and (c-f) CRA-P2OA. Colored bands at the top of each  
 747 picture indicate the weather regime observed for each day: (blue) “NAO<sup>+</sup>” (black) “NAO<sup>-</sup>” (cyan) “Atlantic  
 748 Ridge” and (red) “Blocking”. The gray envelope delimits the extreme values of the daily temperature anomalies  
 749 from the set of analogue days. “an2” indicates the temperature anomalies of the analogue days computed in the  
 750 small domain. Vertical blue dashed lines indicate the 17-20 January 2007 period.



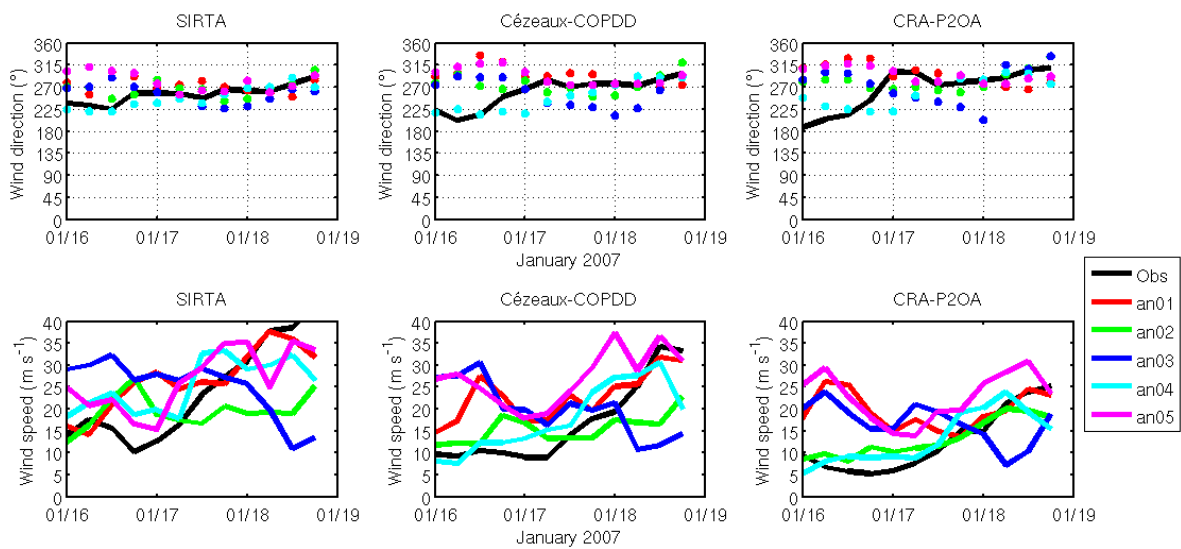
751 FIG. 5. Scatter plots of seasonal correlation coefficients between the large and small domain. The correlation  
 752 coefficients are computed between observed and all analogue day temperature anomalies. Each color represents  
 753 one season: winter (December-February) in black, spring (March to May) in blue, summer (June to August) in  
 754 red and autumn (September to November) in green. The black cross indicates the winter of 2007.



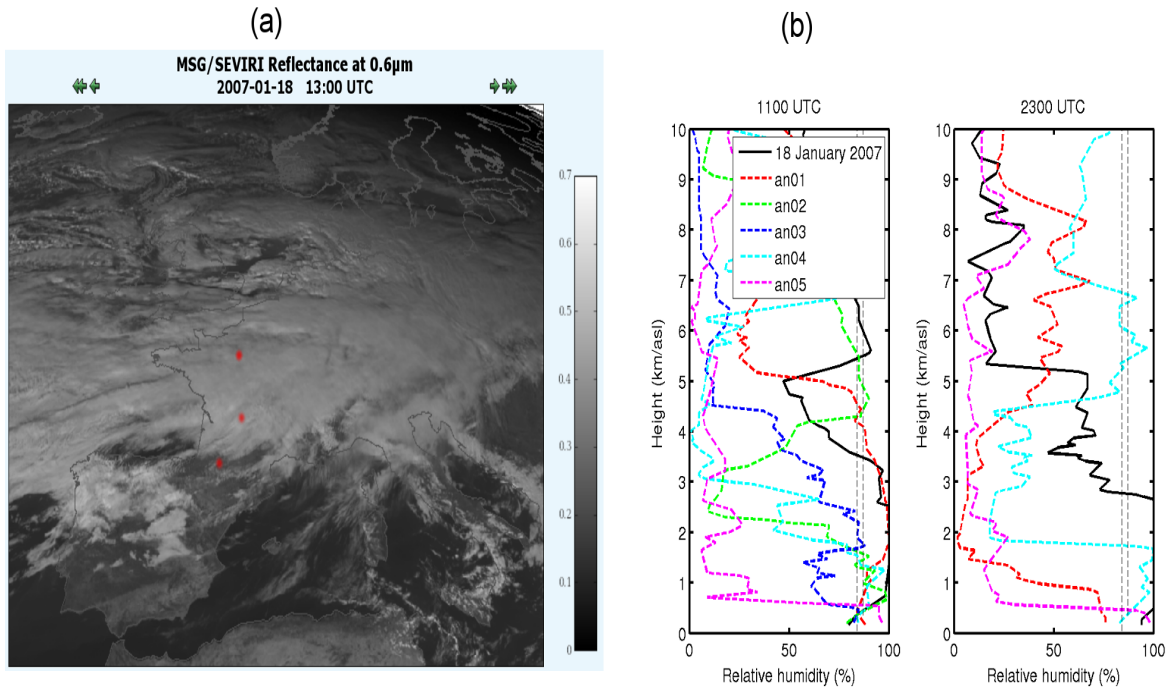
755 FIG. 6. Time series of the monthly normalized index of temperature anomalies observed (red line) and de-  
 756 duced from flow-analogues of the small domain (black line). The vertical dashed lines delimit the four seasons  
 757 of the year (DJF, MAM, JJA, and SON).



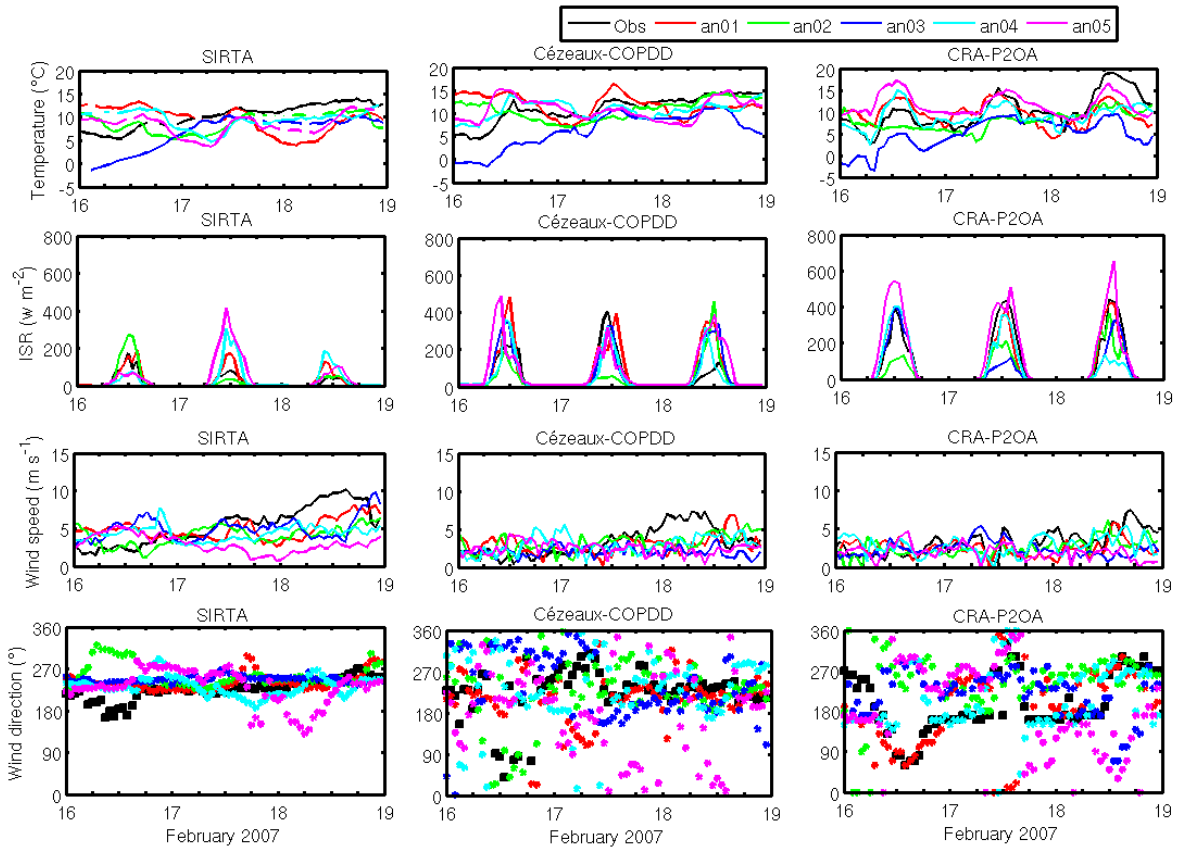
758 FIG. 7. As in Fig. 4, but zoomed in on January-February 2007. Horizontal black segments indicate the two  
 759 specific events analyzed in sections 3.c.1) and 3.c.2). Colored squares at the top of each picture indicate the  
 760 weather regime observed for each day: (blue) “NAO<sup>+</sup>” (black) “NAO<sup>-</sup>” (cyan) “Atlantic Ridge” and (red)  
 761 “Blocking”.



762 FIG. 8. Time series at each site of wind speed and direction for the period from 16 to 18 January 2007 at  
 763 600 mb. The observed series are represented in “black” while the other colors represent the five most accurate  
 764 analogue days for 18 January 2007.



765 FIG. 9. (a) Reflectance in the visible channel of MSG/SEVIRI at  $0.6 \mu\text{m}$  on 18 January 2007 at 1300 UTC.  
 766 This image is available at <http://www.icare.univ-lille1.fr>. Red points in (a) indicate the location of the three  
 767 observatories. (b) Vertical profile of relative humidity at Sirta at 1100 and 2300 UTC, respectively, on 18  
 768 January 2007. Solid lines indicate the observed vertical profiles, while dashed lines represent the five most accu-  
 769 rate analogues. Vertical dashed lines in (b) indicate the minimum (84%) and maximum (87%) relative humidity  
 770 used by Wang and Rossow (1995) to estimate cloud vertical structure: cloud-top and cloud-base heights. No  
 771 radiosoundings at 2300 UTC for the analogue days number 2 and 3.



772 FIG. 10. Time series at each site of the temperature, incoming shortwave radiation (ISR), wind speed and  
 773 direction during the period 16 to 18 January 2007. The observed series are represented in “black”, while the  
 774 other colors represent the historical data of the five most accurate analogue days for 18 January 2007.

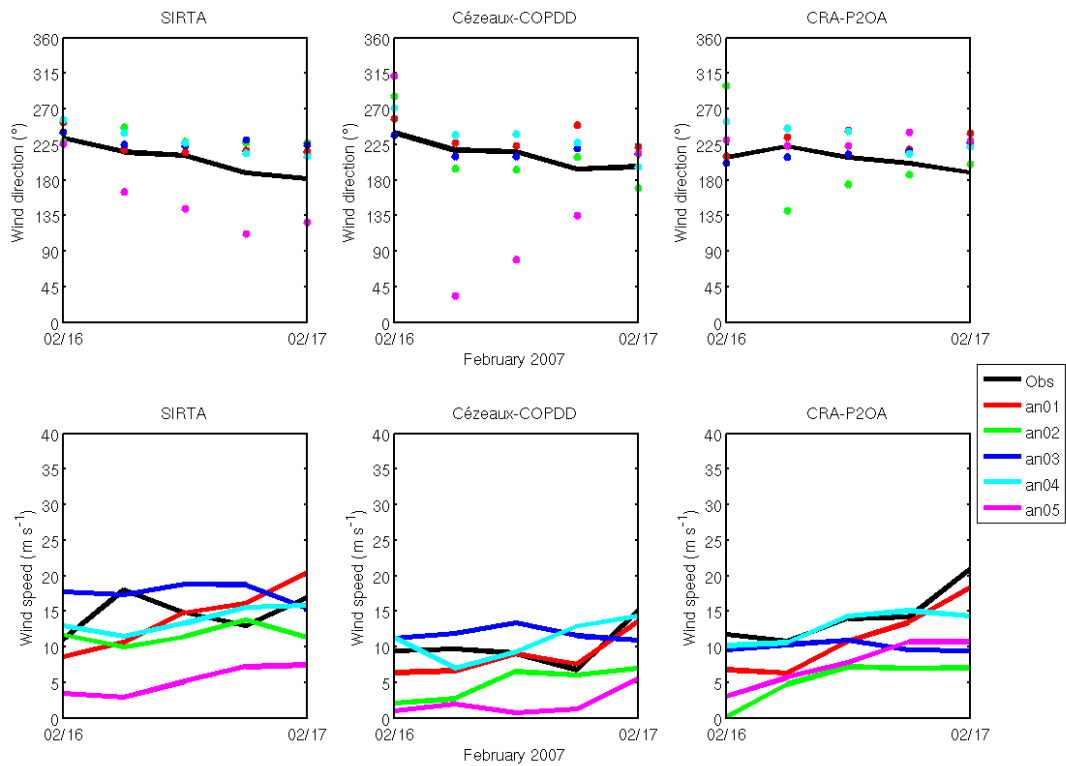
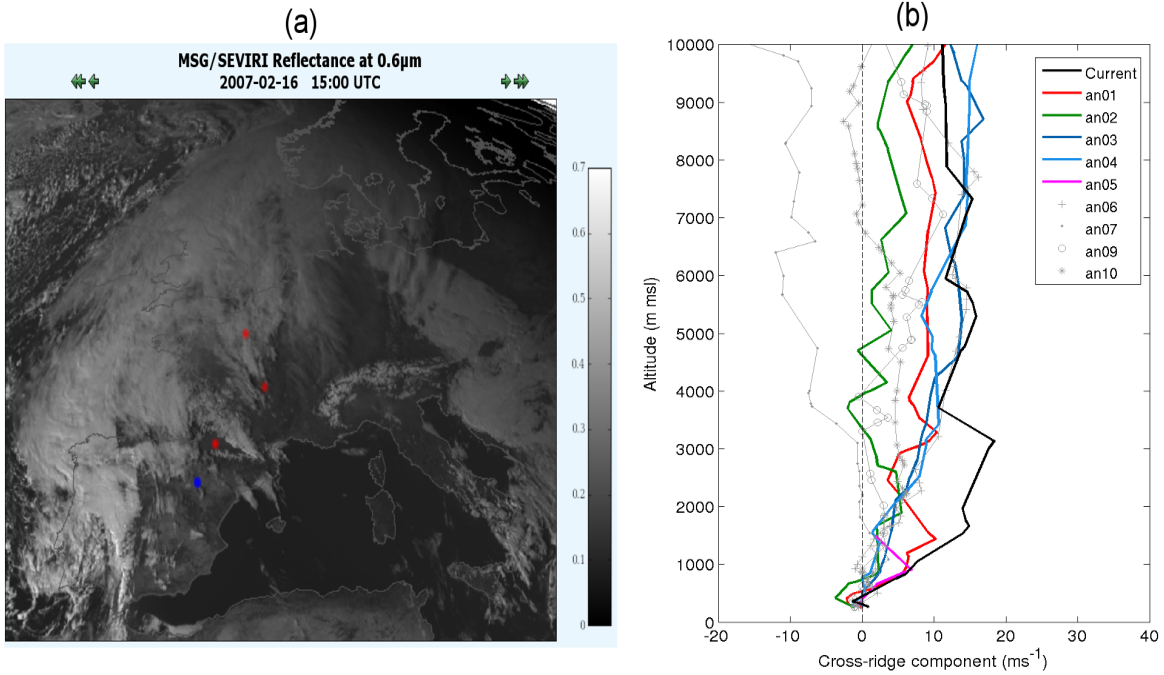


FIG. 11. As in Fig. 8 but for 16 February.



775 FIG. 12. (a) Reflectance in the visible channel of MSG/SEVIRI at  $0.6 \mu\text{m}$  on 16 February 2007 at 1500  
 776 UTC. This image is available at the following site: <http://www.icare.univ-lille1.fr>. Red points in (b) indicate  
 777 the location of the three observatories; the blue point represents the radiosonde station in Zaragosa. (b) Vertical  
 778 profiles of the cross wind component to the Pyrenees ridge ( $210^\circ$ ) observed at Zaragosa, Spain, on 16 February  
 779 and the entirety of its analogues, at 0000 UTC,

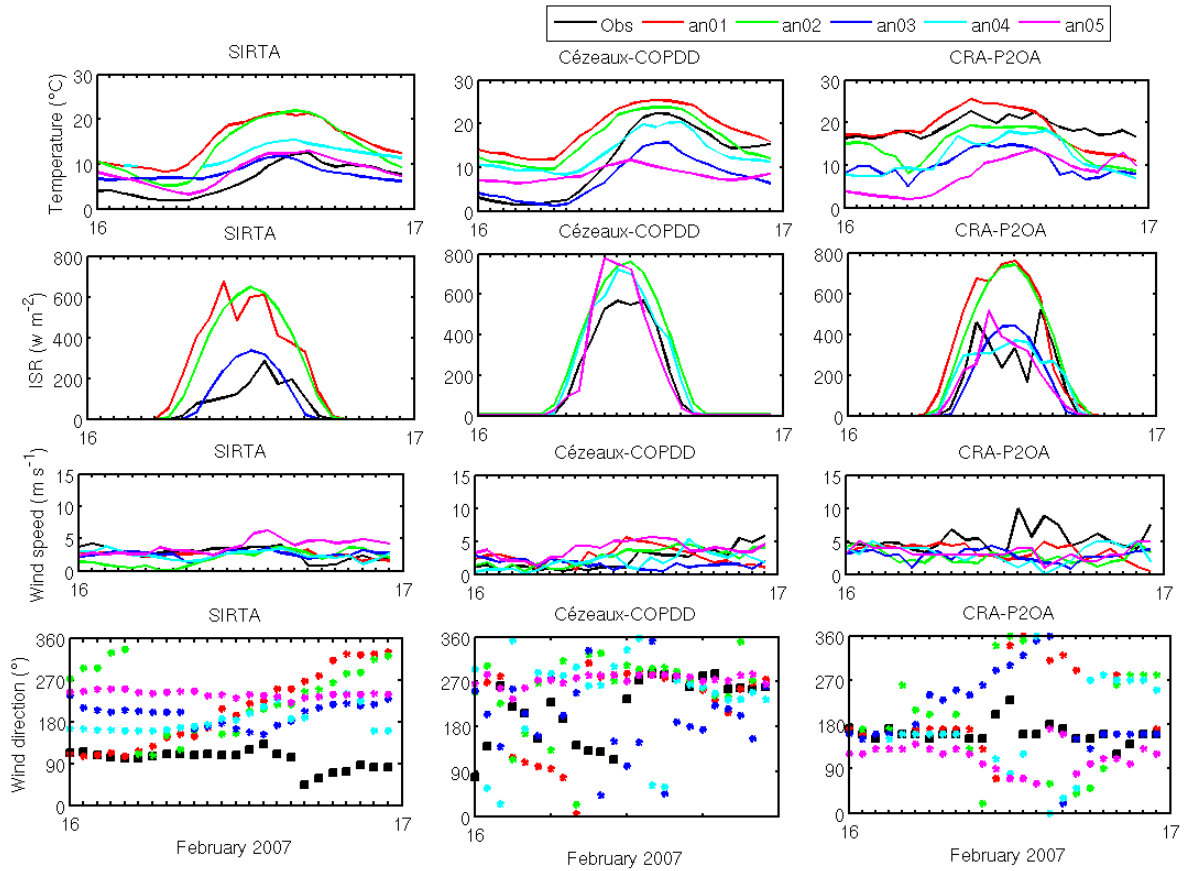


FIG. 13. As in Fig. 10 but for 16 February.